Transient iron coordination sites in proteins: exploiting the dual nature of paramagnetic NMR

Mario Piccioli and Paola Turano*

CERM and Department of Chemistry, University of Florence, via Luigi Sacconi, 6; 50019 Sesto Fiorentino, Italy

Mario Piccioli: piccioli@cerm.unifi.it

Paola Turano: turano@cerm.unifi.it

*Corresponding author:
Paola Turano
CERM
Via Luigi Sacconi, 6
50019 Sesto Fiorentino
Italy
Phone: +39 055 4574266
e-mail: turano@cerm.unifi.it

Abstract

We provide here an historical perspective of NMR applied to iron-containing proteins. At first, the field developed using paramagnetic NMR: the ^{1}H-NMR spectra of heme and FeS proteins were used as clear spectroscopic fingerprints of the electronic structure of the metal ion and its inner and outer coordination spheres. Starting 1994, NMR of metalloproteins was focused more on the protein part and the determination of the 3D structures in solution of small proteins was achieved; paramagnetic NMR observables were exploited as non-conventional NMR constraints. With time, NMR has gained attention as a methodology to monitor protein-protein interactions, becoming a unique tool to learn about the interaction surfaces in weak transient complexes. The recent interest in the understanding of metal ion homeostatis and metal cofactor assembly has led to a renewed interest in the application of NMR: i) as a spectroscopic tool, to characterize the novel binding site of metal centers where the metal is no more an integral part of the protein but rather a chemical entity that has to be transferred along trafficking pathways or a cofactor that has to undergo specific reactions; ii) as a structural method for the definition of the metal-mediated protein-protein interactions. The reported case examples cover the bacterial heme acquisition system, the cytosolic FeS protein assembly and mitochondrial FeS clusters assembly machineries and the eukaryotic iron-storage ferritin.

Keywords: hyperfine interaction, protein-protein interaction, heme acquisition system, iron-sulfur assembly, ferritin.

Table of contents

Abbreviations: FeS, iron-sulfur; CS, contact shift; PCS, pseudocontact shift; RDC^{para}, paramagnetic residual dipolar coupling; CCR, cross correlation; Rdx, rubredoxin; NOE, nuclear Overhauser effect; COSY, correlation spectroscopy, NOESY, nuclear Overhauser effect spectroscopy; HiPIP, high potential iron-sulfur protein; SOD, superoxide dismutase; MW, molecular weight; HSQC, heteronuclear single-quantum correlation; HaS, heme acquisition system; CRINEPT, cross-correlated relaxation-enhanced polarization transfer; TROSY, transverse relaxation-optimized spectroscopy; CIA, cytosolic iron–sulfur protein assembly; FMN, flavin mononucleotide; Grx, glutaredoxin; ISCA, iron-sulfur cluster assembly protein; PCBP, human poly r(C)-binding protein; DPF, diferric-peroxo.

1. Introduction

Iron is essential to virtually all living organism where it's found tightly coordinated in a variety of protein active centers with different functions [1,2]. A crucial distinction is traditionally made between heme and non-heme iron proteins. In heme proteins, iron is stably bound to the porphyrin macrocycle and its coordination sphere is completed by one or two axial ligands; first and second coordination sphere residues modulate function as well as redox and spin states [3]. A bioinformatic analysis of the available structures for non-heme iron-proteins published in 2009 [1] showed that the entire ensemble of non-heme iron proteins in the Protein Data Bank accounts for 86 distinct Fe-sites, more than 50% of which correspond to iron–sulfur centers and about one third to mononuclear centers, the remaining were found to be dinuclear sites, with the only exception of a polynuclear site.

Historically, NMR has contributed to the characterization of two large subsets of iron-proteins: heme and iron sulfur proteins. In all these cases the iron was an integral part of the protein and played a key role for the activity.

To our knowledge, the first spectrum of a heme protein dates back to 1962, when Kowalski [4] published low resolution NMR data on oxidized and reduced horse hearth cytochrome c. Based on the consideration that the ferric cytochrome is paramagnetic and the ferrous form is diamagnetic, he proposed that "*differences in these spectra arise from the change in magnetic properties of the iron"*. In the same years the bases of paramagnetic NMR were established, leading to a well-developed theory that is extensively covered by several books and reviews [5,6,7,8,9,10]; the key concepts and equations are summarized in Section 1.1.

With the exception of low spin iron(II) heme systems, where the large ring current effects produced by the porphyrin macrocycle permit to resolve some of the heme signals outside the diamagnetic envelope, the NMR characterization of iron sites in proteins has been focused on paramagnetic species by exploiting the structural information embedded in the observables which depend on the unpaired electron(s)-nuclear coupling [9].

1.1 Paramagnetic NMR

Nuclei interact with unpaired electrons of metal ions through two main mechanisms: a through-bond contact interaction and a through-space dipolar interaction, which translate into 1) an extra contribution to the nuclear chemical shift (called the hyperfine shift) that adds, with a positive or negative sign, to the diamagnetic shift and 2) a reduction of the nuclear relaxation times [6,11,12,13,14].

1.1.1 Hyperfine shift The hyperfine shift can be estimated by subtracting from the observed shift of the paramagnetic molecule the one measured for a diamagnetic analog. The hyperfine shift is the result of the contact and pseudocontact terms. The relative importance of the two contributions depends on the electronic structure of the paramagnetic metal and on the position of the observed nucleus with respect to the metal center.

The ***contact shift*** (CS) is the through-bond contribution to the hyperfine shift of a nucleus and is proportional to the unpaired electron spin density on the nucleus itself which occurs through direct spin delocalization and/or spin polarization, as expressed by the following Eq. 1.

As such, it's different from zero only for the nuclei of the ligands of the paramagnetic metal ion(s) [15].

$$CS = \frac{A}{\hbar}\frac{\bar{g}\mu_B S(S+1)}{3\gamma_I kT} \quad (1)$$

where *A* is the hyperfine coupling constant, which is proportional to the electron spin density at the nucleus and can be anisotropic due to electron orbital contributions; $\bar{g}$ is the average g value along the principal directions of the contact coupling, when the latter is anisotropic, μ_B is the electron Bohr magneton; *S* is the electron spin number; γ_I is the gyromagnetic ratio of a generic I nucleus; k is the Boltzmann constant; T is the absolute temperature. Hybrid density functional calculations have been used to predict contact shifts for ^{1}H, ^{2}H and ^{13}C spins, in order to confirm NMR assignments and to assess the reliability of calculated spin densities [16]. CS was observed also as the result of unpaired spin delocalization occurring via H-bonds [17].

The **pseudocontact shift** (PCS) originates from the through space, dipolar coupling of the unpaired electron spin with the nuclear spin [18,19]. If the electron magnetic moment is anisotropic (i.e. it has non zero magnetic susceptibility anisotropy), the electron-nuclear dipolar coupling does not average to zero with molecular tumbling in solution and yields a shift that is dependent on both the electron-nucleus distance and the orientation of the electron-nucleus vector with respect to the magnetic susceptibility tensor (Eq. 2). In practice, the mechanism is effective on all the nuclei within a certain distance from the anisotropic paramagnetic metal center and at an appropriate angular position with respect to the magnetic anisotropy tensor axes. PCS is proportional to the inverse third power of the electron-nucleus distance, in the

approximation that the unpaired electron spin density is all metal centered. Given its dependence on distance and angular parameters, PCS provides information on the spatial position of the nucleus with respect to the magnetic axes frame that has the iron in its origin:

$$PCS = \frac{1}{12\pi r_{MH}^3}\left[\Delta\chi_{ax}^{para}(3\cos^2\theta_{MH} - 1) + \frac{3}{2}\Delta\chi_{rh}^{para}(\sin^2\theta_{MH}\cos 2\phi_{MH})\right] \quad (2)$$

Here r_{MH} is the distance of the nucleus H from the metal ion M; $\Delta\chi_{ax}^{para}$ and $\Delta\chi_{rh}^{para}$ are the axial and rhombic components of the anisotropic magnetic susceptibility tensor; θ_{MH} and ϕ_{MH} are the polar angles of the nucleus H with respect to the principal axes of the magnetic susceptibility anisotropy tensor in a reference system that has M in its origin.

1.1.2 Paramagnetic relaxation Coupling between unpaired electron spin(s) and nuclear spins provides them relaxation mechanisms that make nuclear relaxation more efficient, with consequent shortening of **longitudinal and transverse relaxation times** (T_1 and T_2) [13]. The paramagnetic contributions to the nuclear T_1 and T_2 arise from essentially three different sources:

i) The contact interaction, due to delocalized electron spin density and therefore confined to the metal ligands (Eqs. 3 and 4) [20]:

$$T_1^{-1} = \frac{2}{3}\left(\frac{A}{\hbar}\right)^2 S(S+1)\frac{\tau_c}{1+(\omega_I - \omega_S)^2\tau_c^2} \quad (3)$$

$$T_2^{-1} = \frac{1}{3}\left(\frac{A}{\hbar}\right)^2 S(S+1)\left(\frac{\tau_c}{1+(\omega_I - \omega_S)^2\tau_c^2} + \tau_c\right) \quad (4)$$

ii) The electron-nuclear dipolar interaction that, in a metal centered approximation, depends upon the inverse sixth power of the nucleus-iron distance (Eqs. 5 and 6) [21]. When electron spin density is delocalized on the ligand, metal centered approximation does not hold anymore and deviations from Eqs. 5-6 ma be significant. As a general criterion, it has been proposed that only protons farther than four σ bonds, farther than 0.5 nm and not involved in H-bonds to the metal donors should be considered for quantitative interpretations of Eqs. 5-6 [17].

$$T_1^{-1} = \frac{2}{15}\left(\frac{\mu_0}{4\pi}\right)^2 \frac{\gamma_I^2 \mu_B^2 g_e^2 S(S+1)}{r_{MH}^6}\left(\frac{\tau_c}{1+(\omega_I-\omega_S)^2\tau_c^2}+\frac{3\tau_c}{1+\omega_I^2\tau_c^2}+\frac{6\tau_c}{1+(\omega_I+\omega_S)^2\tau_c^2}\right) \quad (5)$$

$$T_2^{-1} = \frac{1}{15}\left(\frac{\mu_0}{4\pi}\right)^2 \frac{\gamma_I^2 \mu_B^2 g_e^2 S(S+1)}{r_{MH}^6}\left(4\tau_C+\frac{\tau_c}{1+(\omega_I-\omega_S)^2\tau_c^2}+\frac{3\tau_c}{1+\omega_I^2\tau_c^2}+\frac{6\tau_c}{1+(\omega_I+\omega_S)^2\tau_c^2}+\frac{6\tau_c}{1+\omega_S^2\tau_c^2}\right) \quad (6)$$

iii) The Curie spin interaction, arising from the interaction between the nuclear spin and the large time-averaged magnetic moment of the electron [22,23]. It also depends upon the inverse sixth power of the metal-nucleus distance. The contribution of this relaxation mechanism to T_1 is negligible, instead the contribution to T_2 becomes dominant at high molecular weights, highly paramagnetic systems and at high magnetic fields (Eq.7):

$$T_2^{-1}(Curie) = \frac{1}{5}\left(\frac{\mu_0}{4\pi}\right)^2 \frac{\omega_I^2 \mu_B^4 g_e^4 S^2(S+1)^2}{(3kT)^2 r_{MH}^6}\left(4\tau_C+\frac{3\tau_c}{1+\omega_I^2\tau_c^2}\right) \quad (7)$$

In equations 3-7, the not-yet defined symbols are: ω_I and ω_S, the Larmor frequencies of the nuclear and electron spins I and S, respectively; γ_I, the gyromagnetic ratio of a generic I nucleus; g_e is the free electron g value. The correlation time for the interactions contributing to the relaxation is indicated by $\tau_{c.}$ and represents the result of various dynamic factors modulating the nuclear-electron spin interaction, each of them characterized by its own correlation time. The relaxation process with the shortest τ becomes dominant, as indicated in Eq. 8:

$$\tau_c^{-1} = \tau_s^{-1} + \tau_r^{-1} + \tau_M^{-1} \qquad (8)$$

where τ_s is the electron relaxation correlation time, τ_r is the rotational correlation time and τ_M is the exchange correlation time that is operative only in the presence of chemical or conformational equilibria. Although in all the equations the same symbol (τ_c) has been used, in the case of contact relaxation (Eqs. 3-4), only chemical exchange (τ_M) and electron relaxation (τ_s) can modulate the coupling between the electron and the nucleus; in the case of dipolar relaxation (Eqs. 5-6) also the rotational correlation time can modulate the interaction. In Curies spin relaxation (Eq. 7), only chemical exchange (τ_M) and rotational correlation (τ_r) are effective.

With the advent of high-field NMR spectrometers new paramagnetic effects have become observable and measurable.

All molecules with molecular magnetic susceptibility anisotropy (χ_{mol}) different from zero adopt preferred orientations in an external magnetic field. The orientation of the molecules in solution follows a Boltzmann distribution and the degree of alignment is proportional to the applied field [24]. This partial alignment gives rise to observable effects in the NMR spectra of

proteins that can be quantified by suitably designed experiments and amplified by addition of orienting media [25]. Among the observables originating from the partial orientation, the non-completely averaged, i.e. residual, dipolar couplings (RDCs) [26,27] are an important source of information. In paramagnetic proteins, when the metal center has non zero magnetic susceptibility anisotropy the molecular magnetic susceptibility is dominated by the paramagnetic contribution (χ_{para}), which is the same magnetic susceptibility responsible of PCS's. As reported in Eq. 9 for the case of the ^{15}N of backbone amide and its attached proton, the **paramagnetic residual dipolar coupling** (RDC^{para}) for a pair of nuclei depends on the orientation of the vector connecting the two nuclei with respect to the magnetic susceptibility tensor axes but, at variance with PCS, not on the distance from the paramagnetic center:

$$RDC^{PARA} = \frac{1}{4\pi}\frac{B_0^2}{15kT}\frac{\gamma_H\gamma_N h}{4\pi^2 r_{NH}^3}\left[\Delta\chi_{ax}^{para}(3\cos^2\theta_{NH}-1)+\frac{3}{2}\Delta\chi_{rh}^{para}(\sin^2\theta_{NH}\cos 2\phi_{NH})\right] \qquad (9)$$

where r_{NH} is the distance between the amide proton and the amide nitrogen and is generally considered fixed; θ_{NH} and ϕ_{NH} are the polar angles that describe the orientation of the internuclear N-H vector with respect to the alignment tensor; γ_N and γ_H are the gyromagnetic ratios of ^{15}N and ^{1}H, respectively; B_0 is the external magnetic field. All the other symbols have the usual meanings.

Cross correlation (CCR) between the internuclear dipolar relaxation and Curie relaxation (see above) causes differential line broadening effects [28,29,30,31,32,33]. In the case of a backbone amide H-N doublet, the effect measured on the ^{1}H spins depends upon the angle between the H-N vector and the H-metal vector and upon the inverse third power of the distance between

the proton and the metal ion and the inverse third power of the distance between the amide proton and the amide nitrogen, taken as fixed (Eq. 10):

$$CCR = \frac{2}{15\pi}\left(\frac{\mu_0}{4\pi}\right)^2 \frac{B_0\gamma_H^2\gamma_N\mu_B^2 g_e^2\hbar S(S+1)}{r_{NH}^3 r_{MH}^3 kT}\left(4\tau_C + \frac{3\tau_c}{1+\omega_0^2\tau_c^2}\right)\frac{(3\cos^2\phi_{CCR}-1)}{2} \qquad (10)$$

Here the only new symbol is ϕ_{CCR} i.e., the angle between the metal-proton vector and the N-H vector.

1.2 NMR of Iron Proteins: an historical perspective.

Besides mononuclear low spin iron(II), all the other iron centers in proteins are paramagnetic, therefore the use of NMR for the characterization of iron proteins has followed over the years the instrumental and methodological developments of paramagnetic NMR. In the quest for a paradigmatic "test" system to address the properties of the hyperfine interaction, heme proteins and Iron-Sulfur proteins have been frequently used. Indeed from the spectroscopic view point, proteins from these two classes are complementary. In heme proteins, the high magnetic anisotropy is such that PCS (Eq. 2) and RDC (Eq. 9) can be extremely informative and indeed, they provide a number of information that can be exploited to obtain structural information (see Section 1.2.2). In FeS proteins, the electron distribution within the cluster is such that the magnetic anisotropy is negligible essentially in all cases. Negligible PCSs remove the problem of factorization between CS and PCS; this has been used to interpret, for nuclei of iron-bound Cys residues, CS contributions in terms of dihedral angle dependence from the dihedral angle Fe-S-C-H, on the basis of a Karplus-type relationship [34]. In both cases, the systems studied for decades were proteins were the iron cofactor was an integral part of the functional form. It is intriguing how, these proteins acted as model systems for more

complicated cases in which transient sites, conformational flexibility, protein-protein interactions complicate the investigation and stimulate, on one hand new methodological development but, on the other hand, the revival of "old" NMR approaches.

1.2.1 Enlightening the metal center. In metalloproteins, NMR signals affected by the interaction with a paramagnetic center can be selectively observed outside the diamagnetic envelope thanks to the hyperfine shift contribution (Eqs. 1 and 2). Typically, the experimental strategy for their observation requires the acquisition of spectra over large spectral windows using fast repetition times, which can be used because of reduced T_1 values (Eqs. 3 and 5) [35,36]. The reduction in T_2 (Eqs. 4, 6 and 7) may cause severe signal broadening and a large number of scans is needed to obtain an acceptable S/N ratio; moreover, signals that are most affected by the paramagnetic center can be broadened beyond detection. According to Eq. 7, the effect is enhanced by the use of high magnetic fields for large molecular weight systems and for systems with high electron spin S values.

The extent of paramagnetic broadening depends upon the nature of the iron center: those with the longest electron relaxation times, τ_s, cause (Eq. 8) the largest reduction in nuclear relaxation times T_1 and T_2 [8,13]. In this frame, iron is the most versatile among all transition metal ions: high spin iron(III) (S=5/2) is one of the most unfavorable ions, having electron relaxation times in the range 10^{-9} – 10^{-11} s, whereas those of low spin iron(III) (S=1/2) and high spin iron(II) (S=2) are of the order of 10^{-11} – 10^{-13} s [37]. Low spin heme iron(III) can be considered as one of the most suitable systems to be studied via paramagnetic NMR because of its particularly favorable τ_s of the order of 10^{-12} s.

The versatility of iron sites in proteins, in terms of electronic properties, oxidation states and coordination chemistry is enhanced by iron ability to form FeS clusters (Fe_2S_2, Fe_3S_4, Fe_4S_4), each of them being available in at least two distinct oxidation states [38,39,40,41]. Within FeS clusters in proteins, iron ions are almost invariantly in a tetrahedral coordination environment provided by two or three inorganic sulfides from the cluster and by one or two sulfur atoms from Cys coordinating residues. Only in the case of Rieske proteins the iron ions of a Fe_2S_2 cluster have asymmetric coordination environments because one of the two iron ions is bound by imidazole Nδ1 atoms of two His residues to form a characteristic Fe(N_2S_2) tetrahedral coordination [42,43,44,45].

In FeS proteins, the electron relaxation time and the spin state of each individual iron ion depends on the magnetic couplings established among iron ions within the FeS cluster and may be substantially different from what expected in the case of Rubredoxins (Rdx), which contain a single $Fe^{3+/2+}$ iron ion bound to four Cys residues in a tetrahedral coordination geometry. Although Rdx's do not contain a FeS cluster nor inorganic sulfur ligands, they are typically considered within the family of FeS proteins. Both iron(III) and iron(II) ions show, in the tetrahedral coordination of Rdx's, long electron relaxation times (ca. 10^{-9} s for iron(III) and ca. 10^{-11}s for iron(II)) and indeed ^{1}H signals from Cys coordinating residues could be observed only in the reduced state at low magnetic field, i.e., under conditions where the Curie term (Eq. 7) is smaller [46]. Rubredoxins represent a nice example on how the direct detection of low γ nuclei such as ^{13}C and ^{15}N may help to characterize paramagnetic centers in proteins. According to Eqs. 6 and 7, paramagnetic relaxation depends on γ^2. When iron-coordinated cysteines are undetectable via ^{1}H NMR spectroscopy because signals are broadened beyond detection, then

low γ (^{13}C, ^{15}N and even ^{2}H) NMR spectroscopy provides extensive assignments for resonances of metal bound residues [47,48,49] (for the advantages of heteronuclear detection in paramagnetic proteins see also section 3.1 and related references).

The magnetic exchange coupling between iron ions in FeS clusters gives rise to paramagnetic centers in which electron relaxation times are always shorter than those of isolated iron ions and new energy levels arise from the combination of the individual S spin states [50,51,52]. The extent of magnetic exchange coupling substantially affects observable NMR parameters [53].

For $[Fe_2S_2]$ containing proteins, in the oxidized state $[Fe_2S_2]^{2+}$, the two iron(III) ions are antiferromagnetically coupled to give a S=0 electronic ground state. Due to the population of excited states of the spin ladder, the protein is paramagnetic at room temperature [50]. Because paramagnetism increases at increasing temperature, hyperfine shifts have a behavior opposed to what expected on the basis of Eq. 1, defined as anti-Curie behavior. The reduced state $[Fe_2S_2]^{+}$, is formally constituted by two iron(III) and one extra electron, for which the localization is driven by the protein environment [54]. In plant-type and human ferredoxins the extra electron is localized and the systems are constituted by one iron(III) and one iron(II) [54] [53]; however delocalized valence was proposed for the bacterial $[Fe_2S_2]$ ferredoxin from *C. pasteurianum [55]* and has been recently observed for the human $[Fe_2S_2]$ protein anamorsin [56].

For $[Fe_4S_4]$ containing proteins, Nature has designed different protein scaffolds that were able to stabilize two out of three possible electronic states: $[Fe_4S_4]^{3+}$, $[Fe_4S_4]^{2+}$, $[Fe_4S_4]^{+}$. The acronym HiPIP (High potential Iron-sulfur Proteins) is used to indicate bacterial proteins in which the

cluster switches between $[Fe_4S_4]^{3+/2+}$, while low potential proteins (ferredoxins) switches between $[Fe_4S_4]^{2+/+}$. In the $[Fe_4S_4]^{2+}$ state, all these systems show a completely delocalized valence in which each iron ion is formally $Fe^{2.5+}$ [57] . The iron ions are pairwise coupled, and give two subspins S=9/2, which are then antiferromagentically coupled to obtain S=0 ground state [58], thus providing a situation similar to what already described in the $[Fe_2S_2]^{2+}$ case [50]. Indeed, both $[Fe_2S_2]^{2+}$ and $[Fe_4S_4]^{2+}$ proteins are EPR silent and have NMR signals with antiCurie behavior [58]. In the $[Fe_4S_4]^{+,}$ state, one of the two iron pair accept the extra electron and become a ferrous pair (S=4). The overall S=1/2 ground state is therefore described as the result of the antiferromagnetic coupling between a mixed valence ion pair with S=9/2 and a pure ferric pair with S=4 [34,59].

A similar behavior is observed in the $[Fe_4S_4]^{3+,}$ state, in which one of the two mixed valence pair of the $[Fe_4S_4]^{2+}$ state loose and electron and become a pure ferric pair [60]. Several HiPIPs have been isolated from photosynthetic bacteria and this has allowed to demonstrate that: i) the iron ion pair delivering the electron when passing from $[Fe_4S_4]^{2+}$ to $[Fe_4S_4]^{3+}$ is not always the same on passing from one HiPIP to another, ii) an equilibrium between two different electronic distributions occurs among all HiPIP [51,61,62,63,64,65,66,67,68]. Overall, HiPIPs provide a demonstration that the electronic properties of the FeS clusters are modulated by the protein environment. Structural differences around the cluster observed even for highly homologous proteins drive the individual oxidation state of each iron ions of the cluster [51,69]. The redox state of the cluster regulates also the thermodynamic stability and triggers protein [70,71]

^{1}H NMR spectra of FeS proteins typically gives rise to spectra in which βCH_2 and αCH protons from Cys residues experience shifts in the range +100/-50 ppm, entirely arising from contact

contributions and, in some case, depend on the Fe-S-C-H dihedral angle [34]. However, both shift and relaxation vary along the various FeS cluster. For example, a $[Fe_4S_4]^{3+}$ cluster is a very favorable systems to be characterized via paramagnetic NMR while a $[Fe_2S_2]^{2+}$ gives rise to much broader NMR lines[39].

Extensive NMR characterization is also available for $[Fe_3S_4]^{+}$ proteins [72,73,74]. The formal symmetry of the system, made by three Fe^{3+} ions, is broken by magnetic coupling: two iron(III) ions couple to obtain a S=2 subspin, the antiferromagnetic coupling between the S=2 pair and an isolated S=5/2 iron(III) gives a total S=1/2 ground state [75,76]. Paramagnetic NMR showed that the Fe^{3+} ion that remains isolated is not always the same. Like the $[Fe_4S_4]$ case, structural factors drive the magnetic coupling scheme [77].

Among mononuclear, non heme, iron sites in proteins that have been studied by NMR, the case of Fe superoxide dismutase (FeSOD) shows how the electron relaxation time of the metal ion is finely tuned by its coordination number. Indeed, iron(III) in the active site of FeSOD is coordinated in a trigonal bipyramid by two His and an Asp in the equatorial plane and by an His and a H_2O molecule in the axial positions. In the reduced, iron(II) form, relatively nice NMR spectra, compared to the case of tetracoordinated iron(II) in Rdx, can be collected, due to the shorter electron relaxation time of pentacoordinated iron(II) with respect to tetracoordinated [78,79]. Paramagnetic NMR also permitted to monitor a structural change in the active site of a tetrameric form of FeSOD (MW about 100 kDa), using variable temperature NMR [80].

In the case of heme proteins, the ^1H heme methyls chemical shift patterns (that arise from a combination of contact and pseudocontact contributions) have soon revealed to constitute a fingerprint of the spin state in iron(III) hemes, allowing a clear discrimination between low spin

(S=1/2) and high spin (S=5/2) spin states, as well as to unravel the presence of intermediate spin form or of spin-admixtures [9]; meso ^{1}H chemical shifts were proposed as probes of the presence of water in the sixth coordination position of iron(III) hemes [81]. Signals of axial ligands in high spin heme iron(III) were generally undetectable (with the exception of the Nδ1 of the proximal His), while they could be observed in the low spin state. The spectra of high spin iron(II) are characterized by less resolved features and therefore most of the research focused on the iron(III) systems, in particular peroxidases in their high spin resting state, metmyoglobin, ferric P450, chlorins and some of their low spin cyanide adducts, ferric cytochromes and spin admixed/intermediate spin cytochromes c'. For an extensive review of this work refer to [9].

The interpretation of the spin delocalization patterns on the porphyrin ring is not trivial and Hückel and density functional theory (DFT) calculations have been employed to this purpose [82,83,84]; in addition, semiempirical equations have been developed for specific combinations of axial ligands in low spin iron(III) heme proteins [85,86] that allow to establish a correlation between chemical shift patterns and axial ligand geometries.

Development of 1D NOE and 2D ^{1}H-^{1}H COSY and NOESY experiments [87,88,89,90,88,91,92,93,94,95,96,97,95] lead to specific assignments of the resonances of heme substituents, of axial ligands (for low spin systems) and of other residues in the heme cavity. These methodological developments in paramagnetic NMR revealed important structure-function relationships: a clear correlation between reduction potential of the heme iron centers and electronic properties modulated via second coordination-sphere effects was established [88,90,98,99,100,101,102], the role of the heme peripheral residues in modulating heme binding preferences was unraveled [88,90,103,104,105,106], mutation of residues in the

distal and proximal cavity helped understanding the role of the conserved amino acids [88,90,100,107,108], the location of small-molecule substrates was identified shading light on the reaction mechanisms [109].

1.2.2 NMR-based solution structures. The first solution structure of a paramagnetic protein was that of the reduced, $[Fe_4S_4]^{2+}$ form of HiPIP I from *Ectothiorhodospira halophila* (Fig. 1) [110,111], solved in 1994 i.e, 10 years after the first application of NMR as a tool for structure determination of diamagnetic proteins [112]. This achievement contradicted common believes [113] that complete solution structures of paramagnetic proteins were not feasible due to the undetectability of residues in the surrounding of the metal; the previous experience in characterizing paramagnetic metal centers in proteins, as described in 1.2.1, was essential to accomplish this goal. This first structure was the beginning of a new era, during which the structure determination of paramagnetic proteins was pursued. These had two major consequences: to move the focus of bioinorganic NMR to smaller proteins such as electron transfer iron-sulfur and cytochromes and to stimulate researchers to exploit the structural information embedded in NMR paramagnetic parameters (see equations 1-10) to derive new structural restraints [10,114].

Among the quantities expressed in Eqs. 1-8 and 10, only PCS, RDC^{para}, CCR, the dipolar term of T_1 and the dipolar and Curie terms of T_2 contain an explicit dependence upon structural parameters such as distances and angles. Different paramagnetic-based NMR restraints have been exploited to refine the structure of different iron proteins, depending on the electronic properties of the metal center.

In the case of FeS proteins, the use of relaxation based-constrains was pursued. For ^{1}H nuclei close to the paramagnetic center, longitudinal relaxation rates are dominated by the term described in Eq. (5) which contains a r^{-6} dependence from the metal-to-nucleus distance and can, therefore, be used as a metal-to-proton structural constraint. T_1 based restraints were used to refine the structure of the HiPIP I from *E. halophila* [115,116] and turned out to be especially relevant in the case of small ferredoxins containing two $[Fe_4S_4]^{2+}$ clusters [117,118]. Indeed, even if the r^{-6} dependence is such that the T_1 based restraints act as short-distance restraints, which usually affect a limited number of protons, in the latter case the small protein size and the presence of two clusters cause a significant percentage of ^{1}H spins experiencing paramagnetic relaxation and therefore the protein structure was substantially improved by the use of relaxation-based NMR constraints. To account for the electron delocalization within the cluster, for each measured T_1 value, the distance to the closest iron ion was considered, and an upper limit value of 5 s^{-1} was considered as diamagnetic contribution to obtain, from the experimental T_1 values, the paramagnetic contribution of Eq. 5 [118].

FeS clusters have a negligible magnetic susceptibility anisotropy and, therefore, relaxation based NMR constraints are the only source of paramagnetic restraints to be possibly exploited. The situation is different in the case of low spin iron(III) paramagnetic heme proteins, where NMR permits to estimate the magnetic susceptibility anisotropy and the principal directions of the magnetic susceptibility tensor axes using the hyperfine shift values measured for the nuclei surrounding the heme, with the exception of those of the coordinating groups [119,120]. In these systems, PCSs (Eq. 2) have been introduced for the first time as non-conventional restraints that complement NOE-based upper distance limits for solution structure

determination (Fig. 2) and used also for the refinement of available crystal structures [121,122,123,124] Later, the measure of PCSs for tens of nuclei (including ^{15}N for backbone amides) has allowed an accurate estimate of the magnetic anisotropy parameters in deoxymyoglobin and reduced cytochrome c' (both high spin iron(II)) [125,126], and in metmyoglobin (high spin iron(III)) [29].

The NMR solution structure determination of paramagnetic metalloproteins with a resolution around the paramagnetic center that is comparable to that of their diamagnetic analogues has allowed to study of the structural changes that accompany variations in the redox state of Iron-sulfur clusters and of heme iron in cytochromes and can be related to the reorganization energy of the electron transfer process [115,122,123,124,127,128,129,130,131,132,133]. The initial steps of the structural biology of heme and iron-sulfur proteins have been reviewed [39,134,135].

In addition to T_1 and PCS, other paramagnetic non-conventional restraints can be derived, which are based on effects detectable only at high magnetic fields. Paramagnetic RDCs (Eq. 9) are constraints that arise from self-orientation induced by a magnetically anisotropic paramagnetic center. As this effect does not depend on the hyperfine interaction but only depends on magnetic anisotropy generated by the metal ions, RDC^{para}'s do not depend at all on the metal-nucleus distance and therefore they are able to provide additional structure information throughout the entire protein. Initially demonstrated in the case of cyano metmyoglobin [26], RDC^{para}'s have been successfully used to refine a large number of other heme proteins, which are invariantly characterized by the presence of strong magnetic anisotropy [26,29,125,136,137,138]. Internal protein motions on the ps to ms time scale can

strongly affect the results: in the presence of internal dynamics the measured RDC values are smaller than expected for a rigid protein with the same structure because they result from the average of all the conformations spanned by the protein in the mentioned time scales. As demonstrated for the alkaline form of cytochrome *c* [136], in the presence of this type of motions, $RDC^{para'}$s are no more useful as structural restraints, but their measure provides information on the dynamics of the system. The use of CCR (Eq. 10), instead is of potential interested but for the moment its use in heme proteins remains a mere exercise [139].

2. Structural biology of iron trafficking. What has been described in the previous Sections summarizes the use of NMR for the characterization of the structure of iron-containing proteins in their isolated forms. More recently, NMR has gained importance as a tool to study interactions involving biological macromolecules. Among the several protein interactions of biological relevance, a large share is composed by the network of protein-protein complexes that regulate metal ions homeostasis and metal cofactors assembly through well-defined trafficking routes. Copper(I) trafficking is the most advanced example of how NMR [140] can contribute to define the interplay between metal coordination chemistry and protein-protein interactions that modulate these fundamental mechanisms. For other metal ions these aspects are less explored. Here we will review some key examples involving iron.

Iron is an essential element: virtually all living organisms require a minimum effective iron concentration of 10^{-8}M. The high toxicity of iron(II) associated to its redox activity and the extremely low solubility of iron(III) species present under aerobic conditions require that iron ions in living systems are found sequestered in high affinity binding proteins. Extracellular iron

is bonded to lactoferrin and transferrin, while intracellular iron (when not in functional iron sites) is stored in the nanocavity of ferritin as an iron-oxo biomineral.

Studying proteins involved in iron uptake and storage requires the definition of the coordination properties that make them able to bind the metal ion with high affinity albeit allowing its release to downstream partners, in response to specific signals. The characterization of these novel iron sites has moved the focus of NMR back on the metal centers, like it was in the 70'es and 80'es, as at the origin of paramagnetic NMR of iron proteins. However, old tools described in 1.2.1 have been flanked by novel approaches, largely based on heteronuclear direct detection, now available thanks to recent technological advancements [141]. Contemporarily, the definition of the determinants of the protein-protein interactions is needed to obtain the complete picture of the process and relies on a new chapter of NMR in structural biology. The main aspects of the use of NMR for protein-protein interactions will be reviewed below; specific approaches developed for our case systems will be discussed in more details in the relevant sections (3.1, 3.2, 3.3).

NMR and protein interactions. NMR is extensively used to monitor protein interactions in solution and to obtain structural information on the resulting adducts. It permits the identification of the protein interfaces and, in some cases, provides intermolecular distance and orientational restraints that lead to the definition of the relative arrangement of the two proteins. In particular, it represents the only structural technique available for studying weak/transient protein–protein interactions, but it can be efficiently used also in the case of strong/stable complexes. By convention, protein-protein complexes are classified in terms of their thermodynamic stability: strong, with dissociation constant K_d for the process $A + B \underset{\rightarrow}{\leftarrow} C$

< 1 μM; weak, with 1 μM < K_d < 100 μM; ultra weak, with K_d > 100 μM [142]. If the recognition process occurs as a one-step reaction (a valid assumption in the absence of large conformational rearrangement upon complex formation), $K_d = k_{off} / k_{on}$, where k_{off} and k_{on} are the dissociation and association rate constants, respectively. A wide range of association rate constants k_{on} has been measured; they are governed by translational diffusion, which is related to the protein size and overall shape, and geometric requirements related to the stereospecific nature of protein-protein complexes (i.e., the two molecules must have appropriate relative orientations when they are in contact). In the absence of long-range intermolecular forces the typical k_{on} values are of the order of 10^5-10^6 $M^{-1}s^{-1}$; when the association process is dominated by electrostatic interaction k_{on} values are generally higher, up to 10^{10} $M^{-1}s^{-1}$ [143,144]. Diffusion-controlled or electrostatic-guided associations typically involve only local conformational changes upon complex formation. When the establishment of an adduct involves gross structural changes such as loop reorganization or domain movement, the association rate constant decreases and k_{on} values are in the range $10^5 > k_{on} > 10^3$ [143]. The dissociation rate constant k_{off} is instead determined by the strength of short range interactions between the interacting proteins and measured values fall in a large interval (10^4-10^{-7} s^{-1}) [145,146]. k_{off} dictates the lifetime of the complex (mean lifetime = $1/k_{off}$; half-life time= $\ln 2/k_{off.}$) [147].

The kinetic aspects of protein-protein interactions are of functional significance: when multiple proteins compete for the same partner or when a protein is faced with alternative pathways, the kinetic control is often the dominant factor and may serve as an additional mechanism for specificity. From the methodological point of view, in NMR k_{on} and k_{off} determine the exchange

rate constant τ_M^{-1} (Eq. 8; often called k_{ex}), which is the crucial parameter for the interpretation of the NMR spectra in binding experiments, through the relation [148]:

$$k_{ex} = k_{on}[A] + k_{off} \quad (11)$$

where [A] is the concentration of the free protein whose spectra are recorded during a titration with the partner molecule B.

If $k_{ex} >> |\Delta\nu|$, (with $\Delta\nu$ being the chemical shift difference, in frequency unit, for a given signal in the free and bound form of A) the system is under the fast exchange regime on the NMR chemical shift time scale and the experimental chemical shift value for a given nucleus will correspond to the population-weighted average of its chemical shift in the bound and free state of the molecule (Fig. 3). Under fast exchange regime, not only the chemical shift, but also all the other NMR parameters result population weighted. When $k_{ex} << |\Delta\nu|$ (slow exchange regime on the NMR chemical shift time scale) two separate signals are observed for the same nucleus, one for the bound and one for the free state of A, with relative intensities that correspond to the relative concentrations of the two states (Fig. 3). At intermediate exchange regimes, signal linewidth is increased due to a phenomenon called “exchange broadening”; such an effect can be so severe to broaden the resonance beyond detection (Fig. 3).

Among the many parameters that can be affected upon complex formation, the chemical shift is the most sensitive indicator of protein-protein interactions and the ^{1}H-^{15}N heteronuclear single-quantum correlation (HSQC) experiment represents the gold standard for monitoring changes in chemical shift involving residues at the protein-protein interface [149,150]. The ^{1}H-^{15}N HSQC, whenever feasible, is an experiment that with cryoprobe technology can be acquired

in a few minutes even for low protein concentrations (down to tens of μM) and the resulting map is a signature of the protein structure. In binding experiments, the ^{1}H-^{15}N HSQC spectrum of one protein in its ^{15}N-enriched form is monitored during the titration with the unlabeled interaction partner. The chemical shift perturbations are recorded for each amino acid; backbone amide proton chemical shifts are very sensitive probes of variations of the chemical environment due to the establishment of the intermolecular interaction and their perturbations give rise to measurable effects even in the case of ultra-weak interactions. Provided the assignment of the ^{1}H-^{15}N HSQC spectrum is available, shift perturbation measurements identify residues of, say, protein A, involved in the interaction with protein B. The weighted average of ^{1}H and ^{15}N chemical shift differences of the backbone amide groups of protein A between the initial and the final stage of a titration, plotted against the residue number provide the so-called Garrett plot [150]. If a structural model of the protein exists, residues undergoing meaningful chemical shift perturbations in the Garrett plot are mapped on the protein structure, thus identifying the interaction area. The procedure can be repeated using ^{15}N-labeled protein B titrated with unlabeled A. Chemical shift perturbation mapping provides the interaction area on the individual binding partners, although does not permit the definition of the relative orientation of the two molecules nor the atom-to-atom interactions at the basis of the recognition process. Residues undergoing chemical shift perturbations can be used as selection filters in data driven computational soft-docking programs [151,152]. In the presence of binding-induced conformational rearrangements, the chemical shift perturbation may extend to residues that are not at the interface, and the chemical shift perturbation fails as a mapping tool, although it still represents an excellent indicator of allosteric processes.

The presence of a paramagnetic species in at least one of the two interacting proteins is a potential source of restraints useful to define the relative orientation of the two proteins, provided the paramagnetic effects extend across the interaction surface. The use of inter-protein PCS has been used for non-functional and functional complexes involving cytochromes (ferricytochrome b_5/ ferricytochrome c and cytochrome f/plastocyanin, respectively) [153] [154]. The use of intermolecular PCS originating from natural heme cofactor suffers for the limited range of action (within 20 Å from the iron center) which may not be sufficient for complexes larger than those composed by two small electron transfer proteins. These limitation has been overcome by introducing on the protein surfaces probes based on caged lanthanides containing strongly anisotropic cations such as ytterbium(III) (with the lutetium(III) derivative acting as a diamagnetic reference) [155].

Paramagnetic Relaxation Enhancements (PRE), based on Eqs. 6 and 7, are another potential source of intermolecular structural restraints, due to their r^{-6} dependence [155,156]. PRE effects on the surface of Zn-rubredoxin originating from high spin iron(III) in the interacting *Desulfovibrio gigas* superoxide reductase have been observed up to 5 Å apart from the paramagnetic center [157]. More efficiently, caged gadolinium(III) engineered on protein surface has been used to monitor protein-protein interactions, leading to the characterization of encounter complexes between electron transfer proteins and in particular involving cytochomes [155,158].

3. Case examples

Here follow three examples of the use of NMR to learn about the bacterial heme acquisition, assembly of the FeS cofactors and iron storage. Each of them has required the development of *ad hoc* methodological approaches that take into account the dynamics and the size of the systems under investigation.

3.1 HasA

Hemophore HasA is a small extracellular protein, with no homology to any other heme binding protein, which is part of the Gram-negative Heme acquisition System (HaS). Its function is to bind free or heme protein-bound heme and to deliver it to a specific outer-membrane receptor, HasR [159]. In vitro, HasA binds heme with a high affinity (*K*a= 5.5×10^{10} M^{-1}), while HasR has a lower affinity for the heme than HasA (*K*a of 5×10^{6} M^{-1}), however, it has been shown that heme is transferred from its binding site on HasA to its binding site on HasR by a protein-protein interaction [160].

As it results from crystal structures [161], in HasA the heme iron(III) ion is bound to an unusual pair of axial ligands: a tyrosine (Tyr75) and a histidine (His32). The Tyr75 oxygen forms a tight hydrogen bond with the Nδ1 of the neighboring His83, that increases the nucleophilic character of Tyr75 and strengthens the Tyr75–iron coordination bond. At variance with the most common heme proteins, the two axial ligands (and His83) belong to two loops that connect the α and β faces of the molecule. These two loops (L1 bearing His32 and L2 bearing Tyr75 and His83) are quite mobile in the apo-form of the protein [162] while close as jaws to trap the heme between them in the holoprotein [161] (Fig. 4). A major challenge in HasA research was to understand

how the peculiar binding site and the structural properties of the protein matrix can induce the release from an apparently higher affinity protein to a lower affinity receptor.

The heme binding site. The ^{1}H heme methyl chemical shift values are diagnostics for the heme iron(III) spin state (Section 1.2.1). In HasA, the ^{1}H NMR data suggest the presence of a non-pure spin state [163]: the average chemical shift for heme methyls (ca. 40 ppm) is, indeed, intermediate between typical values of a purely high-spin, S = 5/2, heme iron(III) and those of a purely low-spin, S = 1/2, heme iron(III); the temperature dependence of the chemical shifts of these signals shows a nonlinear behavior, in contrast with what predicted by Eq. 1. Newly developed ^{13}C direct detection NMR experiments on the wild-type (WT) holoprotein and of mutants in which the three key residues of the active site have been replaced by alanine [164,165], in combination with traditional bulk magnetic susceptibility measurements in solution using the Evans method (see below), provided the key to unravel the nature of the peculiar spectral features of the heme center in HasA.

For any given center with unpaired electrons, paramagnetic relaxation enhancement gives rise to a sphere, centered on the metal ion itself, within which NMR signals are broadened, often beyond detection, due to the effects arising from Eqs. 4, 6 and 7. The radius of such sphere depends on the electron correlation time characteristic of the metal ion, on its spin state, on the size of the molecule and on the magnetic field used for the NMR experiment [13]. However, it depends also on γ^2 and therefore, as already discussed in Section 1.2.1, the direct detection of ^{13}C spins instead of the conventional ^{1}H detection offers the opportunity to s reduce the radius of the “blind sphere” around the paramagnetic center at the expenses of a substantial decrease in sensitivity [166]. The availability of high magnetic field spectrometers equipped

with specific ^{13}C optimized cryo-probes allows one to circumvent the sensibility problem. Actually, all standard ^{1}H detected double and triple resonance experiments have been modified and optimized to work in a ^{13}C, protonless, NMR approach [166]. WT-holo HasA represents a case in which the complete, ^{1}H, ^{13}C and ^{15}N signals assignment was obtained by a combination of standard ^{1}H detected experiments and ^{13}C direct detected experiments [163].

Monodimensional ^{13}C spectra of holo ^{13}C-enriched HasA (with unlabeled heme) allowed us to selectively observe the signals of the axial ligands, which are generally non detectable in ^{1}H spectra of iron(III) heme proteins with S>1/2 (Fig. 5)[163]. The temperature dependence of their chemical shift unambiguously indicated that the structural basis for the non-pure spin state of WT HasA is the release of the axial Y75 ligand upon increasing temperature, which leaves a pentacoordinated species or a six-coordinated species with a water molecule as the sixth ligand. Upon breaking (or weakening) of the coordination bond between the iron and the Tyr, the nuclei of the latter residue would experience no more (or very little) contact shift and therefore their shift will tend towards the diamagnetic value, as observed. At the same time, the signals of the His32 ligand tend toward larger shifts (in absolute value) as expected for axial ligands, when passing from a lower to a higher spin. The H-bond between Tyr75 and H83 has been identified as the determinant of the observed change in axial coordination: in the H83A mutant the ^{1}H and ^{13}C spectra and their temperature are consistent with a pure high spin iron(III) [164]. Monodimensional ^{13}C spectra (Fig.5) have been also the basis of our characterization of Y75A and H32A variants of HasA, because the pattern of hyperfine shifted resonances permits to identify nature and number of axial ligands while their range of chemical shift is diagnostic for the spin state and axial coordination as summarized in Fig. 4 [165]. On the

light of the ^{13}C direct detection data, it was possible to better interpret the heme methyls patterns of ^{1}H spectra. Spin states and presence of water as an axial ligand had been verified using low resolution nuclear magnetic resonance approaches.

Nuclear Magnetic Resonance Dispersion (NMRD) profiles were the key experiment to observe the presence of H_2O in the coordination sphere of mutants where only one axial ligand derived from a protein amino acid, like in H32A [165]. The Evans method, developed in late 50's [167], is a simple approach that, when applied at the newly available high magnetic fields, gives a very sensitive measurement of the spin state of the metal center. The method is based on the measurement of the chemical shift of a probe substance due to the bulk magnetic susceptibility of a solution containing a paramagnetic species, from which a precise measurement of the magnetic moment can be obtained. Evans measurements as a function of temperature have allowed us to discriminate between the temperature-dependent HS-LS spin equilibrium in WT HasA and the S=3/2 configuration characteristic of the Tyr75/H_2O axial coordination in H32A [165].

Surprisingly, although the presence of axial ligands is crucial for the definition of the heme iron spin state, the presence of heme is sufficient to ensure the closed conformation of the two loops, even in absence of the corresponding ligand amino acid, thus demonstrating that second coordination sphere effects between coordinating water molecules and interactions between the porphyrin ring and the protein matrix are stabilizing factors of the closed structure [165]. The structure with unbound His32 (as in H32A) and the one whit broken Tyr75-H83 H-bond (as in H83A) are also relevant for the definition of functional states of the protein-protein complexes that occurs during the heme transfer in the bacterial heme acquisitions system.

Heme-mediated protein-protein interactions. In Nature, the hemophore protein HasA cycles between two states: the heme-bound holoprotein, which functions as a carrier of the metal cofactor toward the membrane receptor HasR, and the heme-free apoprotein fishing for new iron-porphyrin to be taken up from the host organism. Heme release and uptake processes occur via intermediate states characterized by a Tyr75 iron-bound form with open (non-binding) conformation of loop L1. In the case of heme release, a further intermediate state has been proposed: the displacement of His83 causes the breaking of the hydrogen bond with Tys75 and consequent rupture of the coordination bond iron-Tyr. These states do not naturally occur in the WT free protein but can only be driven by the interaction with the partner proteins [165,168,169], as characterized by NMR .

Holo and apo-HasA in solution form a stable complex with HasR solubilized in DPC micelles, giving rise to a stable supramolecular assembly of about 150 kDa [170]. Residues on HasA involved in the interaction with HasR could be identified from ^{1}H-^{15}N CRINEPT-TROSY experiments, which have been developed for the “monolateral” chemical shift mapping of small/medium sized proteins in complexes up to 1 MDa [171]; the proposed interaction area was formed by all signals undergoing changes from their original position in the free form of the hemophore. This lead to the identification of a common contact area for both the holo and the apo-protein. Further information on the conformation adopted by HasA in the complex was derived from the comparison of the ^{1}H-^{15}N fingerprint of all experimentally accessible forms (free apo, free holo, complexed holo and complexed apo). The clear outcome of a distance matrix analysis of the spectral profiles is that only three conformations are accessible to HasA in solution (Fig. 6): that of the isolated holoprotein, that of the isolated apoprotein, and the

conformation in the complex. The latter closely resembles that of the apoprotein and is independent on the presence of the heme in the starting HasA, as heme in the complex is transferred to HasR, with consequent quenching of any paramagnetic effects.

Hemoglobin (Hb) is the main sources of heme in the host organism. The transient interaction between HasA and met-Hb has been studied between the two holo-forms of the proteins [172], because using the biologically relevant pair met-Hb/apo-Has the heme transfer is too fast with respect to the experimental time. Two interaction areas have been identified on HasA: chemical shift perturbations on a fast exchange regime with respect to the NMR chemical shift time scale are localized around the axial ligand Tyr75; line broadening effects interpreted in terms of conformational exchange involve the L1 loop around His32. The latter effect has proposed to originate from "frustrated attempts at changing the conformation of the His32 loop from "closed" to "open" upon sensing the HB surfaces" in this complex where H32 is constrained by the coordination bond with the iron in this non-physiological complex.

3.2 FeS assembly

FeS clusters are probably the oldest and most versatile inorganic cofactors, which can participate in electron transfer, catalysis and regulatory processes [41,173,174,175]. Because inorganic sulfide and ferrous/ferric iron atoms are toxic in vivo, biosynthesis of FeS proteins within cells is a highly regulated process that requires complex protein machineries for the mobilization of Fe and S atoms from appropriate sources, for their assembly and their final delivery to the recipient proteins [176,177,178]. In eukaryotic cells, three distinct FeS protein machineries are operative: the assembly machinery in the mitochondrial matrix, the export

machinery located in the mitochondrial intermembrane space, and the cytosolic iron–sulfur protein assembly (CIA) machinery [179,180]. For proteins involved in these machineries, the situation is quite different from that of small electron transfer proteins such as HiPIP and ferredoxins (discussed in Section 1.2.1 and 1.2.2), which are always monomeric and rigid, thermodynamically very stable and with structural properties tuning the reduction potential of each individual iron ion. In contrast, proteins involved into FeS cluster biogenesis are characterized by flexible structures and by transient states that are driven by the uptake and release of FeS cluster. In these systems the use of old fingerprint approaches for the characterization of the metal center, NMR experiments for solution structure determination and ^{1}H-^{15}N HSQC for protein-protein interactions come together to provide models of the interprotein complexes.

Anamorsin is a protein identified in human CIA machinery. It is a multidomain protein (312 amino acids) characterized by a well folded N-Term domain, an unstructured linker of about 50 aminoacid residues and a C-term region, called CIAPIN1 domain, that binds a [Fe_2S_2] cluster [181]. This protein receives electrons from a diflavin reductase Ndor1 [182]. The electron transfer complex between Ndor1 and anamorsin has been monitored via ^{1}H-^{15}N HSQC experiments performed upon ^{15}N labeling of one of the two interacting proteins, according to the protocol described in Section 2. Specific protein-protein recognition between a completely unstructured region involving the linker and part of the C-term of anamorsin and a α-helical containing face of the FMN binding domain of Ndor1 is observed from these experiments (Fig. 7) [183]. The formation of the stable complex is independent of the presence of the Fe_2S_2 center as well of the redox state of the FMN moiety, indicating that the two partners do

interact permanently and no dissociation occurs along the electron transfer process. This molecular recognition involves regions that are not in direct contact with the redox cofactors; once the complex is formed, the areas surrounding FMN and the Fe_2S_2 redox centers transiently interact indicating that an electron transfer over a short distance is still possible in multiple orientation without the requirement to format specific interaction between the two redox centers [183], in analogy to the encounter complexes described in Section 2.

Paramagnetic NMR was fundamental to unravel the structure of the CIAPIN1 domain, the 108-amino acid C-terminal domain of anamorsin. Indeed, the CIAPIN1 domain is largely unstructured and contains paramagnetic Fe_2S_2 center. About 30% of HN resonances are unobserved in a standard HSQC experiment due to the presence of the Fe_2S_2 center. To identify HN resonances from residues within a, roughly, 10 Å distance from each of the two iron ions, a new HSQC experiment has been designed and applied to the isolated CIAPIN1 domain [184]. With this approach, thirteen resonances previously unobserved could be identified (Fig. 8), assigned and the measured ^1H T_1 values could be used as restraints to define the protein environment of the cluster in the CIAPIN1 domain.

A similar combination of experiments has been used also to monitor the cluster transfer between mitochondrial monothiol Glutaredoxin 5 (Grx5)[185,186], that contains a [Fe_2S_2] cluster, and ISCA1, a iron-sulfur cluster assembly protein that is required for the maturation of mitochondrial [Fe_4S_4] proteins [187,188]. The problem is the understanding, at the molecular level, of the transfer of [Fe_2S_2] from Grx5 to ISCA1.

Established NMR methods to map protein-protein interactions were consistent with a cluster transfer occurring via an associative process involving specific protein-protein interactions.

NMR structures and relaxation measurements of apo- and holo Grx5 show that cluster binding induces a change of Grx5 quaternary structure passing from an apo monomer to a holodimer [189]. Paramagnetic NMR was the only method to identify Grx5 residues belonging to the proximity of the cluster. Monodimensional ^{1}H and ^{13}C experiments (Fig 9 A) unambiguously showed the presence of two forms of the holoprotein, which are very similar in terms of hyperfine contributions to both chemical shift and nuclear relaxation but behave differently during the protein-protein interaction. HSQC experiments indicated that one of the two holoGrx5 forms is more reactive than the other with respect to transferring the $[Fe_2S_2]$ cluster to apo Isca1. The structural switch between two conformational states observed in holo Grx5 could be a general mechanism used by monothiol glutaredoxins in FeS assembly pathways(Fig. 9B), that would permit Grx5 to efficiently release the cluster to multiple protein partners [189].

3.3 Ferritin

Ferritins are the main iron storage proteins in eukaryotes and prokaryotes; about 30% of the total iron in a healthy human is found stored within ferritin [190,191]. These proteins formed by 24 subunits that self-assemble in highly symmetric nanocage architecture, with total molecular mass of the order of 480 kDa. The protein shell surrounds a central cavity that occupies about 1/3 of the total volume of the molecule and which can store up to 4500 iron atoms in the form of a ferric-oxo mineral. The sequence of the subunits varies from one organism to another and, in eukaryotes, one ferritin molecule may be formed by multiple types of subunits. All subunits, however, share a 4-helix bundle structure completed, on one side of the bundle, by a short C-terminal helix H5. (Fig. 10). The symmetry of the overall architecture

derives from *i*) extended intersubunit contacts involving pairs of helices with head-to-tail relative orientation (C2 symmetry axes), *ii*) contacts among the H5 helices of 4 different subunits that create 6 pores with C4 symmetry and *iii*) contacts among 3 subunits that come together via the side of the bundle opposite to the H5 helix to form 8 ion channels with C3 symmetry.

The overall reaction occurring in ferritin is [191]:

$$2Fe^{2+} + O_2 + (H_2O)_{x+3} \rightarrow Fe_2O_3(H_2O)_x + 4H^+ + H_2O_2$$

In practice, it proceeds through a multisetp process that requires iron(II) entering the protein shell, reaching the active center of catalytic subunits, where it is oxidized to diferric iron products, and then migrating towards the nanocavity to generate the biomineral, that is released in response to specific stimuli. The X-ray structure of the protein part is known at high resolution for ferritins from many organisms [192,193,194], but the interaction mode of iron with the protein was not defined until very recently, with an important contribution from NMR [195].

There are several unanswered or only-partially answered questions in ferritin chemistry: The interactome of ferritin is largely unknown. Human Poly r(C)-Binding Proteins 1-3 (PCBP1-3) have been proposed to function as cytosolic iron chaperones in the delivery of iron to ferritin [196], and direct interactions between the chaperons and ferritin have been recently reported on the basis of ITC experiments [197]. There are no evidences that a protein-protein interaction is at the basis of the iron release from the biomineral, although it's known that synthetic peptides may facilitate the process [198].

The role of C4 pores is not well-understood. They have a hydrophobic surface and contain residue that, in crystal structures, are shown to interact with metal ions [199], but the available variants with mutations of such residues do not show significantly different iron uptake and only slightly different iron release [200]. On the contrary, negatively charged residues in the C3 pores have a crucial role in iron uptake, as shown by mutation studies where Asp and Glu binding metal cations in X-ray structures have been substituted with hydrophobic side chains [200,201,202,203]. Unfolding of the C3 pores facilitates iron release [204,205].

The mechanism of the catalytic reaction occurring at ferritin active is still matter of debate. The subunits of prokaryotic ferritins and the so-called H and M subunits of eukaryotic ferritin are catalytically functional: upon addition of iron(II) in ferritin solution a diferric-peroxo (DPF) intermediate forms (with typical absorbance at 650 nm) and quickly evolves into ferric-oxo species (monitored at 350 nm) [206]. Based on these observations it had been proposed that two ferrous ions react with O_2 at the catalytic site forming the DPF intermediate and immediately after transform in diferric-oxo dimers that migrate towards the nanocavity to form the biomineral, leaving an empty active site that would be ready to host two new incoming iron(II) ions in a subsequent reaction turnover [207]. X-ray structure solved in the presence of redox-inactive divalent cations such as zinc(II) and magnesium(II) where taken as models of the ferrous-bound precursors; small differences in the coordination sphere where interpreted as the key to determine whether the Fe-active site bonds persist throughout the reaction cycle (in diiron enzymes, where iron is the catalytic center) or break to release diferric oxo products (in ferritin, where iron(II) is the reaction substrate) [208].

This was the generally accepted scenario when we decided to study the ferritin reaction by NMR. Structure-function relationships can be derived from NMR experiments only if at least a partial NMR assignment of the protein spectra is available. The ferritin size prevents the use of standard solution NMR approaches for sequence specific assignments; as detailed in references [195,209]. ^{1}H NMR lines for slow tumbling molecules above 100 kDa are prohibitively large for triple resonance experiments. ^{13}C NMR spectra have a better resolution, at least for aliphatic and Cα nuclei, but assignment strategies based on protonless pulse sequences also failed due to the short transverse relaxation times that do not allow efficient coherence transfer in J-coupled experiments. On the other hand ^{13}C-^{13}C NOESY maps allowed the detection of well resolved spin-patterns for most of the amino acid side chains, thus constituting an ideal starting point for monitoring the reaction between the protein and partner molecules/ions in solution [210,211]. We therefore developed a combined solution/solid state NMR approach in which solid state NMR experiments of ferritin microcrystals were successful to obtain sequence specific assignments, which then could be used to exploit solution state ^{13}C-^{13}C NOESY maps (Fig. 11) [209]. This was the basis for the characterization of the ferritin-iron interaction in solution. Iron was added with a stoichiometry of two iron(II) ions per ferritin subunit and the obtained ^{13}C-^{13}C NOESY map was compared with that of the apoprotein: according to the common beliefs we would have expected to observe signal broadening due to paramagnetic effects arising from the diferric-oxo products inside the nanocavity. Instead paramagnetic broadening beyond detection was observed for residues in the middle of the 4-helix bundle channel in the proximity of the magnesium/zinc binding sites (Fig. 12 A and B) [209]. The two ferric ions are antiferromagnetically coupled with apparent effective magnetic moment of 4.5

μ_B, as measured by Evans experiments.[209] The expected paramagnetic broadening in a 480 kDa protein at high magnetic field is dominated by the Curie relaxation (Eq. 7) and is expected, at 16.4 T, to broaden beyond detection residues within about 5 Å from the metal ions. Using the signals of assigned isoleucine residues (which are well resolved in ^{13}C-^{13}C NOESY and strategically distributed in the protein structure) as probes of the location of the paramagnetic species we could establish that the diferric products remains stably bound at the catalytic center after the oxidation reaction as occurred and that the binding site is close but not coincident with that of the redox inactive cations observed in the X-ray structures [209]. To further confirm this result that was contrasting previous views, we have solved the X-ray structures of iron-loaded ferritin crystals obtained by soaking crystals in $FeSO_4$ solutions followed by flash freezing: the binding site of diferric species was thus unequivocally defined (Fig. 12 C) [199], although a debate is still open on the mechanism the ferric ions are replaced by new incoming iron(II) species in subsequent turnovers [195,212,213]. The pathway guiding the ferric products formed at the active site towards the cavity need to be precisely defined. NMR titrations of ferritin with iron were conducted with subsequent additions of iron(II) in steps of two ions/subunit (up to 8 irons/subunit). While the paramagnetic effects observed in ^{13}C-^{13}C NOESY with the first two irons/subunit persist, the number of signals broadened beyond detection increases at each step, with affected residues located between the active site and the H5 helix, toward the C4 pore (Fig. 12 B) [209]. The obvious interpretation of these data is as follows: new incoming iron(II) ions substitute the di-iron(III) moiety at the catalytic site and are oxidized in subsequent turnovers; the ferroxidase center is always occupied by iron; a push-pull mechanism induced by the new ferrous iron forces the leaving diferric products to proceeds

towards the nanocavity through a pathway involving residues between the active site and the C4 term of the bundle. Evans measurements suggested antiferromagnetic coupling between subsequently formed diferric products that probably generate increasingly larger clusters [209]. The latter mechanism still waits to be proved by higher resolution data.

Acknowledgements. We acknowledge the Bio-NMR Project (Contract 261686) and MIUR-PRIN2009 for financial support.

References

[1] C. Andreini, I. Bertini, G. Cavallaro, R. J. Najmanovich, J. M. Thornton, J.Mol.Biol. 388 (2009) 356-380.

[2] I. Bertini, A. Sigel, H. Sigel, Handbook on Metalloproteins, Marcel Dekker, 2001.

[3] P. Turano, Y. Lu, in: I. Bertini, A. Sigel, H. Sigel (Eds.), Handbook on Metalloproteins, Marcel Dekker, NY, 2001, pp. 269-356.

[4] A. Kowalsky, J Biol.Chem. 237 (1962) 1807-1819.

[5] D. R. Eaton, R. D. Fischer, C. J. Hawkins, W. D. Horrocks, Jr., J. P. Jesson, R. W. Kreilick, R. J. Kurland, G. N. La Mar, C. H. Langford, W. D. Phillips, L. H. Pignolet, M. F. Rettig, T. J. Swift, NMR of Paramagnetic Molecules, Academic Press, 1973.

[6] I. Bertini, C. Luchinat, NMR of paramagnetic molecules in biological systems, Benjamin/Cummings, 1986.

[7] I. Bertini, C. Luchinat, NMR of paramagnetic substances, Coord.Chem.Rev. 150, Elsevier, 1996.

[8] I. Bertini, C. Luchinat, G. Parigi, Solution NMR of paramagnetic molecules, Elsevier, 2001.

[9] I. Bertini, P. Turano, A. J. Vila, Chem.Rev. 93 (1993) 2833-2932.

[10] I. Bertini, C. Luchinat, M. Piccioli, Methods Enzymol. 339 (2001) 314-340.

[11] I. Bertini, C. Luchinat, M. Mancini, G. Spina, in: D. Gatteschi, O. Kahn, R. D. Willett (Eds.), Magneto-structural correlations in exchange-coupled systems, Reidel Publishing Company, Dordrecht, 1985, pp. 421-461.

[12] I. Bertini, L. Banci, C. Luchinat, in: N. J. Oppenheimer, T. L. James (Eds.), Nuclear Magnetic Resonance, Part B, Methods Enzymol., Vol. 177, London, 1989, pp. 246-246.

[13] L. Banci, I. Bertini, C. Luchinat, Nuclear and electron relaxation. The magnetic nucleus-unpaired electron coupling in solution, VCH, 1991.

[14] I. Bertini, C. Luchinat, R. Pierattelli, in: C. I. Stassinopoulou (Eds.), NMR of biological macromolecules. NATO ASI Series., Springer-Verlag, Berlin, 1994, pp. 199-216.

[15] H. M. McConnell, D. B. Chesnut, J.Chem.Phys. 28 (1958) 107-117.

[16] S. J. Wilkens, B. Xia, F. Weinhold, J. L. Markley, W. M. Westler, J.Am.Chem.Soc. 120 (1998) 4806-4814.

[17] S. J. Wilkens, W. M. Westler, J. L. Markley, J.Am.Chem.Soc. 120 (1998) 4893-4894.

[18] H. M. McConnell, R. E. Robertson, J.Chem.Phys. 29 (1958) 1361-1365.

[19] R. J. Kurland, B. R. McGarvey, J.Magn.Reson. 2 (1970) 286-301.

[20] N. Bloembergen, J.Chem.Phys. 27 (1957) 575-596.

[21] I. Solomon, Phys.Rev. 99 (1955) 559-565.

[22] M. Gueron, J.Magn.Reson. 19 (1975) 58-66.

[23] A. J. Vega, D. Fiat, Mol.Phys. 31 (1976) 347-355.

[24] A. A. Bothner-By, J. P. Domaille, C. Gayathri, J.Am.Chem.Soc. 103 (1981) 5602-5603.

[25] J. H. Prestegard, C. M. Bougault, A. I. Kishore, Chem.Rev. 104 (2004) 3519-3540.

[26] J. R. Tolman, J. M. Flanagan, M. A. Kennedy, J. H. Prestegard, Proc.Natl.Acad.Sci.USA 92 (1995) 9279-9283.

[27] A. Bax, N. Tjandra, J.Biomol.NMR 10 (1997) 289-292.

[28] I. Bertini, C. Luchinat, M. Piccioli, D. Tarchi, Concepts Magn.Reson. 6 (1994) 307-335.

[29] P. Turano, G. Battaini, L. Casella, Chem.Phys.Lett. 373 (2003) 460-463.

[30] G. Pintacuda, K. Hohenthanner, G. Otting, N. Muller, J.Biomol.NMR 27 (2003) 115-132.

[31] J. Boisbouvier, P. Gans, M. Blackledge, B. Brutscher, D. Marion, J.Am.Chem.Soc. 121 (1999) 7700-7701.

[32] I. Bertini, G. Cavallaro, M. Cosenza, R. Kümmerle, C. Luchinat, M. Piccioli, L. Poggi, J.Biomol.NMR 23 (2002) 115-125.

[33] F. Kateb, M. Piccioli, J.Am.Chem.Soc. 125 (2003) 14978-14979.

[34] I. Bertini, F. Capozzi, C. Luchinat, M. Piccioli, A. J. Vila, J.Am.Chem.Soc. 116 (1994) 651-660.

[35] T. Inubushi, E. D. Becker, J.Magn.Reson. 51 (1983) 128-133.

[36] L. Banci, I. Bertini, C. Luchinat, M. Piccioli, A. Scozzafava, P. Turano, Inorg.Chem. 28 (1989) 4650-4656.

[37] I. Bertini, C. Luchinat, G. Parigi, R. Pierattelli, ChemBioChem 6 (2005) 1536-1549.

[38] I. Bertini, C. Luchinat, in: D. M. Grant, R. K. Harris (Eds.), Encyclopedia of Magnetic Resonance, John Wiley & Sons, Ltd, Chicester, 1996, pp. 2621-2625.

[39] C. Luchinat, F. Capozzi, D. Bentrop, in: I. Bertini, A. Sigel, H. Sigel (Eds.), Handbook on Metalloproteins, Marcel Dekker, 2001, pp. 357-460.

[40] W. R. Hagen, Adv.Inorg.Chem. 38 (1992) 165-222.

[41] D. C. Johnson, D. R. Dean, A. D. Smith, M. K. Johnson, Annu.Rev.Biochem. 74 (2005) 247-281.

[42] J. A. Fee, K. L. Findling, T. Yoshida, R. Hille, G. E. Tarr, D. O. Hearshen, W. R. Dunham, E. P. Day, T. A. Kent, E. Munck, J.Biol.Chem. 259 (1984) 124-133.

[43] J. Meyer, J. Gagnon, J. Gaillard, M. Lutz, C. Achim, E. Munck, Y. Petillot, C. M. Colangelo, R. A. Scott, Biochemistry 36 (1997) 13374-13380.

[44] K. L. Hsueh, W. M. Westler, J. L. Markley, J.Am.Chem.Soc 132 (2010) 7908-7918.

[45] K. L. Hsueh, M. Tonelli, K. Cai, W. M. Westler, J. L. Markley, Biochemistry 52 (2013) 2862-2873.

[46] M. T. Werth, D. M. Kurtz, Jr., I. Moura, J. LeGall, J.Am.Chem.Soc. 109 (1987) 273-275.

[47] I. J. Lin, B. Xia, D. S. King, T. E. Machonkin, W. M. Westler, J. L. Markley, J.Am.Chem.Soc. 131 (2009) 15555-15563.

[48] I. J. Lin, E. B. Gebel, T. E. Machonkin, W. M. Westler, J. L. Markley, Proc.Natl Acad.Sci., USA 102 (2005) 14581-14586.

[49] B. Xia, W. M. Westler, H. Cheng, J. Meyer, J.-M. Moulis, J. L. Markley, J.Am.Chem.Soc. 117 (1995) 5347-5350.

[50] L. Banci, I. Bertini, C. Luchinat, Struct.Bonding 72 (1990) 113-135.

[51] L. Banci, I. Bertini, S. Ciurli, S. Ferretti, C. Luchinat, M. Piccioli, Biochemistry 32 (1993) 9387-9397.

[52] I. Bertini, S. Ciurli, C. Luchinat, Struct.Bonding 83 (1995) 1-54.

[53] B. Xia, D. Jenk, D. M. LeMaster, W. M. Westler, J. L. Markley, Archives of Biochemistry and Biophysics 373 (2000) 328-334.

[54] L. B. Dugad, G. N. La Mar, L. Banci, I. Bertini, Biochemistry 29 (1990) 2263-2271.

[55] C. Achim, E. L. Bominaar, J. Meyer, J. Peterson, E. Munck, J.Am.Chem.Soc. 121 (1999) 3704-3714.

[56] L. Banci, S. Ciofi-Baffoni, M. Mikolajczyk, J. Winkelmann, E. Bill, M. Eirini Pandelia, J.Biol.Inorg.Chem. 18 (2013) 883-893.

[57] P. Middleton, D. P. E. Dickson, C. E. Johnson, J. D. Rush, Eur.J.Biochem. 104 (1980) 289-296.

[58] I. Bertini, F. Briganti, C. Luchinat, A. Scozzafava, M. Sola, J.Am.Chem.Soc. 113 (1991) 1237-1245.

[59] G. Blondin, J.-J. Girerd, Chem.Rev. 90 (1990) 1359-1376.

[60] L. Banci, I. Bertini, F. Briganti, C. Luchinat, A. Scozzafava, M. Vicens Oliver, Inorg.Chem. 30 (1991) 4517-4524.

[61] D. G. Nettesheim, T. E. Meyer, B. A. Feinberg, J. D. Otvos, J.Biol.Chem. 258 (1983) 8235-8239.

[62] D. G. Nettesheim, S. R. Harder, B. A. Feinberg, J. D. Otvos, Biochemistry 31 (1992) 1234-1244.

[63] I. Bertini, F. Capozzi, S. Ciurli, C. Luchinat, L. Messori, M. Piccioli, J.Am.Chem.Soc. 114 (1992) 3332-3340.

[64] I. Bertini, F. Capozzi, C. Luchinat, M. Piccioli, M. Vicens Oliver, Inorg.Chim.Acta 198-200 (1992) 483-491.

[65] L. Banci, I. Bertini, F. Capozzi, P. Carloni, S. Ciurli, C. Luchinat, M. Piccioli, J.Am.Chem.Soc. 115 (1993) 3431-3440.

[66] L. Banci, I. Bertini, S. Ferretti, C. Luchinat, M. Piccioli, J.Mol.Struct. 292 (1993) 207-220.

[67] I. Bertini, F. Capozzi, C. Luchinat, M. Piccioli, Eur.J.Biochem. 212 (1993) 69-78.

[68] I. Bertini, F. Capozzi, L. D. Eltis, I. C. Felli, C. Luchinat, M. Piccioli, Inorg.Chem. 34 (1995) 2516-2523.

[69] S. G. Iwagami, A. L. Creagh, C. A. Haynes, M. Borsari, I. C. Felli, M. Piccioli, L. D. Eltis, Protein Sci. 4 (1995) 2562-2572.

[70] I. Bertini, J. A. Cowan, C. Luchinat, K. Natarajan, M. Piccioli, Biochemistry 36 (1997) 9332-9339.

[71] D. Bentrop, I. Bertini, R. Iacoviello, C. Luchinat, Y. Niikura, M. Piccioli, C. Presenti, A. Rosato, Biochemistry 38 (1999) 4669-4680.

[72] D. Bentrop, I. Bertini, C. Luchinat, J. Mendes, M. Piccioli, M. Teixeira, Eur.J.Biochem. 236 (1996) 92-99.

[73] A. L. Macedo, I. Moura, J. J. G. Moura, J. LeGall, B. H. Huynh, Inorg.Chem. 32 (1993) 1101-1105.

[74] K. Nagayama, D. Ohmori, Y. Imai, T. Oshima, FEBS Lett. 158 (1983) 208-212.

[75] T. A. Kent, B. H. Huynh, E. Munk, Proc.Natl.Acad.Sci.USA 77 (1980) 6574-6576.

[76] D. Bentrop, I. Bertini, M. Borsari, G. Cosenza, C. Luchinat, Y. Niikura, Angew.Chem.Int.Ed 39 (2000) 3620-3622.

[77] S. C. Busse, G. N. La Mar, L. P. Yu, J. B. Howard, E. T. Smith, Z. H. Zhou, M. W. W. Adams, Biochemistry 31 (1992) 11952-11962.

[78] L.-J. Ming, J. B. Lynch, R. C. Holz, L. Que, Jr., Inorg.Chem. (1994) 83-87.

[79] C. K. Vance, A. F. Miller, Biochemistry 37 (1998) 5518-5527.

[80] J. P. Renault, I. Morgenstern-Badarau, M. Piccioli, Inorg.Chem. 38 (1999) 614-615.

[81] B. A. Springer, S. G. Sligar, Proc.Natl.Acad.Sci.USA 84 (1987) 8961-8965.

[82] N. V. Shokhirev, F. A. Walker, JBIC 3 (1998) 581-594.

[83] M. D. Liptak, X. Wen, K. L. Bren, J.Am.Chem.Soc. 132 (2010) 9753-9763.

[84] Kumar A., P. C. Mshra, C. S. Verma, V. Renugopalakrishnan, Int.J.Quantum Chem. 102 (2005) 1002-1009.

[85] I. Bertini, C. Luchinat, G. Parigi, F. A. Walker, J.Biol.Inorg.Chem. 4 (1999) 515-519.

[86] N. V. Shokhirev, F. A. Walker, J.Am.Chem.Soc. 120 (1998) 981-990.

[87] R. D. Johnson, S. Ramaprasad, G. N. La Mar, J.Am.Chem.Soc. 105 (1983) 7205-7206.

[88] S. W. Unger, J. T. J. Lecomte, G. N. La Mar, J.Magn.Reson. 64 (1985) 521-526.

[89] L. P. Yu, G. N. La Mar, K. Rajarathnam, J.Am.Chem.Soc. 112 (1990) 9527-9534.

[90] V. Thanabal, J. S. de Ropp, G. N. La Mar, J.Am.Chem.Soc. 110 (1988) 3027-3035.

[91] J. S. de Ropp, L. P. Yu, G. N. La Mar, J.Biomol.NMR 1 (1991) 175-190.

[92] K. A. Keating, J. S. de Ropp, G. N. La Mar, A. L. Balch, F.-Y. Shiau, K. M. Smith, Inorg.Chem. 30 (1991) 3258-3263.

[93] M. Sette, J. S. de Ropp, G. Hernandez, G. N. La Mar, J.Am.Chem.Soc. 115 (1993) 5237-5245.

[94] J. S. de Ropp, G. N. La Mar, J.Am.Chem.Soc. 113 (1991) 4348-4350.

[95] I. Bertini, F. Capozzi, C. Luchinat, P. Turano, J.Magn.Reson. 95 (1991) 244-252.

[96] L. Banci, I. Bertini, P. Turano, M. Vicens Oliver, Eur.J.Biochem. 204 (1992) 107-112.

[97] L. Banci, I. Bertini, C. Luchinat, L. Messori, P. Turano, Appl.Magn.Reson. 4 (1993) 461-476.

[98] L. Banci, I. Bertini, P. Turano, M. Tien, T. K. Kirk, Proc.Natl.Acad.Sci.USA 88 (1991) 6956-6960.

[99] L. Banci, I. Bertini, E. A. Pease, M. Tien, P. Turano, Biochemistry 31 (1992) 10009-10017.

[100] J. C. Ferrer, P. Turano, L. Banci, I. Bertini, I. K. Morris, K. M. Smith, M. Smith, A. G. Mauk, Biochemistry 33 (1994) 7819-7829.

[101] L. Banci, I. Bertini, I.-C. Kuan, M. Tien, P. Turano, A. J. Vila, Biochemistry 32 (1993) 13483-13489.

[102] J. Bujons, A. Dikiy, J. C. Ferrer, L. Banci, A. G. Mauk, Eur.J.Biochem. 243 (1997) 72-84.

[103] K.-B. Lee, E. Jun, G. N. La Mar, I. N. Rezzano, R. K. Pandey, F. A. Walker, D. H. Buttlaire, J.Am.Chem.Soc. 113 (1991) 3576-3583.

[104] K.-B. Lee, G. N. La Mar, R. K. Pandey, I. N. Rezzano, K. E. Mansfield, K. M. Smith, T. C. Pochapsky, S. G. Sligar, Biochemistry 30 (1991) 1878-1887.

[105] G. N. La Mar, J. B. Hauksson, L. B. Dugad, P. A. Liddell, N. Venkataramana, K. M. Smith, J.Am.Chem.Soc. 113 (1991) 1544-1550.

[106] R. E. Berry, D. Muthu, T. K. Shokhireva, S. A. Garrett, A. M. Goren, H. Zhang, F. A. Walker, J.Biol.Inorg.Chem. Epub ahead of print (2013)

[107] L. P. Yu, G. N. La Mar, Biochemistry 29 (1990) 2578-2585.

[108] P. Turano, J. C. Ferrer, M. R. Cheesman, A. J. Thomson, L. Banci, I. Bertini, A. G. Mauk, Biochemistry 34 (1995) 13895-13905.

[109] L. Banci, I. Bertini, T. Bini, M. Tien, P. Turano, Biochemistry 32 (1993) 5825-5831.

[110] L. Banci, I. Bertini, L. D. Eltis, I. C. Felli, D. H. W. Kastrau, C. Luchinat, M. Piccioli, R. Pierattelli, M. Smith, Eur.J.Biochem. 225 (1994) 715-725.

[111] I. Bertini, I. C. Felli, D. H. W. Kastrau, C. Luchinat, M. Piccioli, M. S. Viezzoli, Eur.J.Biochem. 225 (1994) 703-714.

[112] M. P. Williamson, D. Marion, K. Wuthrich, J.Mol.Biol. 173 (1984) 341-359.

[113] G. Wagner, Progr.NMR Spectrosc. 22 (1990) 101-139.

[114] F. Arnesano, L. Banci, M. Piccioli, Q Rev Biophys 38 (2005) 167-219.

[115] I. Bertini, L. D. Eltis, I. C. Felli, D. H. W. Kastrau, C. Luchinat, M. Piccioli, Chem.Eur.J. 1 (1995) 598-607.

[116] I. Bertini, M. M. J. Couture, A. Donaire, L. D. Eltis, I. C. Felli, C. Luchinat, M. Piccioli, A. Rosato, Eur.J.Biochem. 241 (1996) 440-452.

[117] I. Bertini, A. Donaire, B. A. Feinberg, C. Luchinat, M. Piccioli, H. Yuan, Eur.J.Biochem. 232 (1995) 192-205.

[118] I. Bertini, A. Donaire, C. Luchinat, A. Rosato, Proteins Struct.Funct.Genet. 29 (1997) 348-358.

[119] K. Rajarathnam, G. N. La Mar, M. L. Chiu, S. G. Sligar, J.Am.Chem.Soc. 114 (1992) 9048-9058.

[120] L. Banci, I. Bertini, R. Pierattelli, M. Tien, A. J. Vila, J.Am.Chem.Soc. 117 (1995) 8659-8667.

[121] L. Banci, I. Bertini, K. L. Bren, M. A. Cremonini, H. B. Gray, C. Luchinat, P. Turano, J.Biol.Inorg.Chem. 1 (1996) 117-126.

[122] L. Banci, I. Bertini, K. L. Bren, H. B. Gray, P. Sompornpisut, P. Turano, Biochemistry 36 (1997) 8992-9001.

[123] L. Banci, I. Bertini, H. B. Gray, C. Luchinat, T. Reddig, A. Rosato, P. Turano, Biochemistry 36 (1997) 9867-9877.

[124] M. Assfalg, L. Banci, I. Bertini, M. Bruschi, P. Turano, Eur.J.Biochem. 256 (1998) 261-270.

[125] I. Bertini, C. Luchinat, P. Turano, G. Battaini, L. Casella, Chem.Eur.J. 9 (2003) 2316-2322.

[126] P. Tsan, M. Caffrey, M. L. Daku, M. Cusanovich, D. Marion, P. Gans, J.Am.Chem.Soc. 121 (1999) 1795-1805.

[127] P. Baistrocchi, L. Banci, I. Bertini, P. Turano, K. L. Bren, H. B. Gray, Biochemistry 35 (1996) 13788-13796.

[128] L. Banci, I. Bertini, M. Bruschi, P. Sompornpisut, P. Turano, Proc.Natl.Acad.Sci.USA 93 (1996) 14396-14400.

[129] M. Assfalg, L. Banci, I. Bertini, M. Bruschi, M. T. Giudici-Orticoni, P. Turano, Eur.J.Biochem. 266 (1999) 634-643.

[130] L. Banci, I. Bertini, J. G. Huber, G. A. Spyroulias, P. Turano, J.Biol.Inorg.Chem. 4 (1999) 21-31.

[131] L. Brennan, D. L. Turner, A. C. Messias, M. L. Teodoro, J. LeGall, H. Santos, A. V. Xavier, J.Mol.Biol. 298 (2000) 61-82.

[132] C. A. Salgueiro, D. L. Turner, A. V. Xavier, Eur.J.Biochem. 244 (1997) 721-734.

[133] T. C. Pochapsky, M. Kostic, N. Jain, R. Pejchal, Biochemistry 40 (2001) 5602-5614.

[134] L. Banci, I. Bertini, C. Luchinat, P. Turano, in: K. M. Kadish, K. M. Smith, R. Guilard (Eds.), The Porphyrin Handbook, Academic Press, San Diego, CA, 2000, pp. 323-350.

[135] F. Arnesano, L. Banci, I. Bertini, F. Capozzi, S. Ciurli, C. Luchinat, S. Mangani, S. Ciofi-Baffoni, A. Rosato, P. Turano, M. S. Viezzoli, Coord.Chem.Rev. 250 (2006) 1419-1450.

[136] M. Assfalg, I. Bertini, P. Turano, A. G. Mauk, J. R. Winkler, B. H. Gray, Biophys.J. 84 (2003) 3917-3923.

[137] L. Banci, I. Bertini, J. G. Huber, C. Luchinat, A. Rosato, J.Am.Chem.Soc. 120 (1998) 12903-12909.

[138] F. Arnesano, L. Banci, I. Bertini, K. van der Wetering, M. Czisch, R. Kaptein, J.Biomol.NMR 17 (2000) 295-304.

[139] L. Banci, I. Bertini, G. Cavallaro, A. Giachetti, C. Luchinat, G. Parigi, J.Biomol.NMR 28 (2004) 249-261.

[140] L. Banci, I. Bertini, S. Ciofi-Baffoni, HFSP J. 3 (2009) 165-175.

[141] I. C. Felli, A. Piai, R. Pierattelli, Ann.Rep.NMR Spectroscop. (2013) 359-418.

[142] A. J. Rowe, Methods 54 (2011) 157-166.

[143] G. Schreiber, G. Haran, H. X. Zhou, Chem.Rev. 109 (2009) 839-860.

[144] R. Alsallaq, H. X. Zhou, Proteins: Struct., Funct., Bioinf. 71 (2008) 320-335.

[145] M. Prudencio, M. Ubbink, J.Mol.Recognit. 17 (2004) 524-539.

[146] A. I. Archakov, V. M. Govorun, A. V. Dubanov, Y. D. Ivanov, A. V. Veselovsky, P. Lewi, P. Janssen, Proteomics 3 (2003) 380-391.

[147] J. Corzo, Biochem.Mol.Biol.Educ. 34 (2006) 413-416.

[148] C. A. Lepre, J. M. Moore, J. W. Peng, Chem.Rev. 104 (2004) 3641-3675.

[149] J. Vaynberg, J. Qin, Trends in Biotechnology 24 (2006) 22-27.

[150] D. S. Garrett, Y. J. Seok, A. Peterkofsky, G. M. Clore, A. M. Gronenborn, Biochemistry 36 (1997) 4393-4398.

[151] S. J. de Vries, A. D. van Dijk, M. Krzeminski, M. van Dijk, A. Thureau, V. Hsu, T. Wassenaar, A. M. Bonvin, Proteins: Struct., Funct., Bioinf. 69 (2007) 726-733.

[152] C. Dominguez, R. Boelens, A. M. Bonvin, J.Am.Chem.Soc. 125 (2003) 1731-1737.

[153] R. D. Guiles, S. Sarma, R. J. DiGate, D. Banville, V. J. Basus, I. D. Kuntz, L. Waskell, Nature Struct.Biol. 3 (1996) 333-339.

[154] R. Hulsker, M. V. Baranova, G. S. Bullerjahn, M. Ubbink, J.Am.Chem.Soc. 130 (2008) 1985-1991.

[155] M. Prudencio, J. Rohovec, J. A. Peters, E. Tocheva, M. J. Boulanger, M. E. Murphy, H. J. Hupkes, W. Koster, A. Impagliazzo, M. Ubbink, Chem.Eur.J. 5 (2004) 3252-3260.

[156] P. H. J. Keizers, M. Ubbink, Prog.Nucl.Magn Reson.Spectrosc. 58 (2011) 88-96.

[157] R. M. Almeida, P. Turano, I. Moura, G. L. C. Moura, S. R. Pauleta, ChemBioChem 14 (2013) 1858-1866.

[158] M. Ubbink, Biochem.Soc.Trans. 40 (2012) 415-418.

[159] J. M. Ghigo, S. Letoffe, C. Wandersman, J.Bacteriol. 179 (1997) 3572-3579.

[160] N. Izadi-Pruneyre, F. Huché, G. S. Lukat-Rodgers, A. Lecroisey, R. Gilli, K. R. Rodgers, C. Wandersman, P. Delepelaire, J.Biol.Chem. 281 (2006) 25541-25550.

[161] P. Arnoux, R. Haser, N. Izadi, A. Lecroisey, M. Delepierre, C. Wandersman, M. Czjzek, Nat.Struct.Biol. 6 (1999) 516-520.

[162] N. Wolff, N. Izadi-Pruneyre, J. Couprie, M. Habeck, J. Linge, W. Rieping, C. Wandersman, M. Nilges, M. Delepierre, A. Lecroisey, J.Mol.Biol. 376 (2008) 517-525.

[163] C. Caillet-Saguy, M. Delepierre, A. Lecroisey, I. Bertini, M. Piccioli, P. Turano, J.Am.Chem.Soc. 128 (2006) 150-158.

[164] C. Caillet-Saguy, P. Turano, M. Piccioli, G. Lukat-Rodgers, M. Czjzek, B. Guigliarelli, N. Izadi-Pruneyre, K. Rodgers, M. Delepierre, A. Lecroisey, J.Biol.Chem. 283 (2008) 5960-5970.

[165] C. Caillet-Saguy, M. Piccioli, P. Turano, G. Lukat-Rodgers, N. Wolff, K. Rodgers, N. Izadi-Pruneyre, M. Delepierre, A. Lecroisey, J.Biol.Chem. 287 (2012) 26932-26943.

[166] W. Bermel, I. Bertini, I. C. Felli, M. Piccioli, R. Pierattelli, Progr.NMR Spectrosc. 48 (2006) 25-45.

[167] D. F. Evans, J.Chem.Soc. (1959) 2003-2005.

[168] G. Jepkorir, J. C. Rodriguez, H. Rui, W. Im, S. Lovell, K. P. Battaille, A. Y. Alontaga, E. T. Yukl, P. Moenne-Loccoz, M. Rivera, J.Am.Chem.Soc. 132 (2010) 9857-9872.

[169] E. T. Yukl, G. Jepkorir, A. Y. Alontaga, L. Pautsch, J. C. Rodriguez, M. Rivera, P. Moenne-Loccoz, Biochemistry 49 (2010) 6646-6654.

[170] C. Caillet-Saguy, M. Piccioli, P. Turano, N. Izadi-Pruneyre, M. Delepierre, I. Bertini, A. Lecroisey, J.Am.Chem.Soc. 131 (2009) 1736-1744.

[171] J. Fiaux, E. B. Bertelsen, A. L. Horwich, K. Wüthrich, Nature 418 (2002) 207-211.

[172] A. Y. Alontaga, J. C. Rodriguez, E. Schönbrunn, A. Becker, T. Funke, E. T. Yukl, T. Hayashi, J. Stobaugh, P. Moënne-Loccoz, M. Rivera, Biochemistry 48 (2009) 96-109.

[173] H. Beinert, R. H. Holm, E. Munck, Science 277 (1997) 653-659.

[174] R. Lill, Nature 460 (2009) 831-838.

[175] J. Meyer, J.Biol.Inorg.Chem. 13 (2008) 157-170.

[176] M. Fontecave, S. Ollagnier-de-Choudens, Arch.Biochem.Biophys. 474 (2008) 226-237.

[177] R. Lill, U. Muhlenhoff, Annu.Rev.Biochem. 77 (2008) 669-700.

[178] S. S. Mansy, J. A. Cowan, Acc.Chem.Res. 37 (2004) 719-725.

[179] R. Lill, U. Muhlenhoff, Annu.Rev.Cell Dev.Biol. 22 (2006) 457-486.

[180] T. A. Rouault, Nat.Chem.Biol. 2 (2006) 406-414.

[181] L. Banci, I. Bertini, S. Ciofi-Baffoni, F. Boscaro, A. Chatzi, M. Mikolajczyk, K. Tokatlidis, J. Winkelmann, Chem.Biol. 18 (2011) 794-804.

[182] D. J. Netz, M. Stumpfig, C. Dore, U. Muhlenhoff, A. J. Pierik, R. Lill, Nat.Chem.Biol. 6 (2010) 758-765.

[183] L. Banci, I. Bertini, V. Calderone, S. Ciofi-Baffoni, A. Giachetti, D. Jaiswal, M. Mikolajczyk, M. Piccioli, J. Winkelmann, Proc.Natl.Acad.Sci.U.S.A 110 (2013) 7136-7141.

[184] S. Ciofi-Baffoni, A. Gallo, R. Muzzioli, M. Piccioli, J.Biomol.NMR, in press

[185] C. H. Lillig, C. Berndt, A. Holmgren, Biochim.Biophys.Acta 1780 (2008) 1304-1317.

[186] P. Shakamuri, B. Zhang, M. K. Johnson, J.Am.Chem.Soc. 134 (2012) 15213-15216.

[187] K. D. Kim, W. H. Chung, H. J. Kim, K. C. Lee, J. H. Roe, Biochem.Biophys.Res.Commun. 392 (2010) 467-472.

[188] U. Muhlenhoff, N. Richter, O. Pines, A. J. Pierik, R. Lill, J.Biol.Chem. 286 (2011) 41205-41216.

[189] L. Banci, S. Ciofi-Baffoni, R. Del Conte, R. Gadepalli, M. Mikolajczyk, S. Neri, M. Piccioli, J. Winkelmann (2015)

[190] E. C. Theil, R. K. Behera, T. Tosha, Coord.Chem.Rev. 257 (2013) 579-586.

[191] X. Liu, E. C. Theil, Acc.Chem.Res. 38 (2005) 167-175.

[192] R. R. Crichton, J. P. Declercq, Biochim Biophys Acta 1800 (2010) 706-718.

[193] K. J. Cho, H. J. Shin, J. H. Lee, K. J. Kim, S. S. Park, Y. Lee, C. Lee, S. S. Park, K. H. Kim, J Mol Biol 390 (2009) 83-98.

[194] A. Marchetti, M. S. Parker, L. P. Moccia, E. O. Lin, A. L. Arrieta, F. Ribalet, M. E. Murphy, M. T. Maldonado, E. V. Armbrust, Nature 457 (2009) 467-470.

[195] D. Lalli, P. Turano, Acc.Chem.Res. 46 (2013) 2676-2685.

[196] H. Shi, K. Z. Bencze, T. L. Stemmler, C. C. Philpott, Science 320 (2008) 1207-1210.

[197] S. Leidgens, K. Z. Bullough, H. Shi, M. Shakoury-Elizeh, T. Yabe, P. Subramanian, E. Hsu, N. Natarajan, A. Nandal, T. L. Stemmler, C. C. Philpott, J.Biol.Chem. 288 (2013) 17791-17802.

[198] X. S. Liu, L. D. Patterson, M. J. Miller, E. C. Theil, J.Biol.Chem. 282 (2007) 31821-31825.

[199] I. Bertini, D. Lalli, S. Mangani, C. Pozzi, C. Rosa, E. C. Theil, P. Turano, J.Am.Chem.Soc. 134 (2012) 6169-6176.

[200] E. C. Theil, P. Turano, M. Allegrozzi, V. Ghini, C. Bernacchioni, J.Biol.Inorg.Chem. (2014)

[201] S. Haldar, L. E. Bevers, T. Tosha, E. C. Theil, J.Biol.Chem. 286 (2011) 25620-25627.

[202] T. Tosha, R. K. Behera, E. C. Theil, Inorg.Chem. 51 (2012) 11406-11411.

[203] X. Yang, P. Arosio, N. D. Chasteen, Biophys.J. 78 (2000) 2049-2059.

[204] T. Tosha, R. K. Behera, H. L. Ng, O. Bhattasali, T. Alber, E. C. Theil, J Biol.Chem. 287 (2012) 13016-13025.

[205] H. Takagi, D. Shi, Y. Ha, N. M. Allewell, E. C. Theil, J.Biol.Chem. 273 (1998) 18685-18688.

[206] J. Hwang, C. Krebs, B. H. Huynh, D. E. Edmondson, E. C. Theil, J. E. Penner-Hahn, Science 287 (2000) 122-125.

[207] J. K. Schwartz, X. S. Liu, T. Tosha, E. C. Theil, E. I. Solomon, J.Am.Chem.Soc. 130 (2008) 9441-9450.

[208] T. Tosha, M. R. Hasan, E. C. Theil, Proc.Natl.Acad.Sci.U.S.A 105 (2008) 18182-18187.

[209] P. Turano, D. Lalli, I. C. Felli, E. C. Theil, I. Bertini, Proc.Natl.Acad.Sci.USA 107 (2010) 545-550.

[210] W. Bermel, I. Bertini, I. C. Felli, M. Matzapetakis, R. Pierattelli, E. C. Theil, P. Turano, J.Magn.Reson. 188 (2007) 301-310.

[211] M. Matzapetakis, P. Turano, E. C. Theil, I. Bertini, J.Biomol.NMR 38 (2007) 237-242.

[212] K. H. Ebrahimi, E. Bill, P. L. Hagedoorn, W. R. Hagen, Nat.Chem.Biol. 8 (2012) 941

[213] K. H. Ebrahimi, P. L. Hagedoorn, W. R. Hagen, ChemBioChem 14 (2013) 1123-1133.

Figure captions

Fig. 1. The first solution structure of a paramagnetic protein: family of the 15 best structures of the reduced form of high-potential iron-sulfur protein I from *Ectothiorhodospira halophila*, containing a $[Fe_4S_4]^{2+}$ cluster [110].

Fig. 2. First application of PCS for structural refinement: the solution structure of the cyanide adduct of Ala80cytochrome c determined via NOE-based upper distance limits (top panel) has been refined using PCS restraints (lower panel) taking advantage of the large magnetic susceptibility anisotropy of the low spin heme-iron(III) center [121].

Fig.3. Exchange regimes on the chemical shift NMR time scale in binding experiments. When a nucleus experience two distinct chemical environments in the free and bound form of a molecule, different situations are possible depending on the relative value of k_{ex} and on the difference in chemical shift (expressed in frequency units) of the two forms. When passing from the slow (top trace) to the fast exchange (bottom trace), we observe signal broadening and coalescence into a single resonance.

Fig. 4. The holo HasA structure and the heme binding module in WT and mutants. Top left: the ribbon representation of the protein structure highlights the segregated α (magenta) and β (orange) regions, loop L1 bearing the H32 axial ligand (green), loop L2 (bearing the axial ligand Y75 and the H-bonded H32; both cyan); the heme is represented by ball-and-sticks. Top-right: the spectroscopic features of WT holoHasA are consistent with a thermally-dependent equilibrium between a low-spin and a high-

spin form. Bottom, from left to right: axial coordination and spin state at neutral pH of Y75A, H83A and H32A.

Fig. 5. Monitoring the axial ligation of HasA variants by ^{13}C NMR. The monodimensional ^{13}C NMR spectra of WT HasA and its mutants reflect the difference in the number of axial ligands provided by protein amino acids (number of detectable resonances) and spin state (chemical shift range).

Fig. 6. NMR fingerprint of HasA conformations. ^{1}H-^{15}N spectral fingerprint of holo and apoHasA in their free form and when bound to HasR have been analyzed using a distance matrix approach. Three main conformations have been observed and here indicated by three different colors: the open form of apoHasA (dark green), the closed form of holoHasA (brownish red), and a common complexed form (light green). The latter is much closer to that of apoHasA (0.54/0.55) than to the holoHasA (1.00). The numbers are the results of the statistical spectral comparison; a value of zero corresponds to identity while an index on 1 is attributed to the pair resulting in the largest difference.

Fig. 7. Binding interface of the FMN-binding domain of Ndor1 interacting with $[Fe_2S_2]$-anamorsin. Residues experiencing chemical shift and line broadening variations upon interaction are indicated with spheres. Chemical shift changes occurs at the Ndor1 regions involved in the encounter complex with anamorsin, line broadening effects are observed as a consequence of the proximity of the paramagnetic $[Fe_2S_2]$ center. Large blue spheres: residues showing large chemical shift changes and characterized by relative solvent accessibility above 50%. Small blue spheres: residues showing large

chemical shift changes but featuring relative solvent accessibility lower than 50%. Large cyan spheres: residues showing small chemical shift changes with concomitant broadening effects and with relative solvent accessibility above 50%. Small cyan spheres: residues showing small chemical shift changes with concomitant broadening effects and with relative solvent accessibility lower than 50%. Positively charged (gray), negatively charged (red), and hydrophobic (yellow) side chains which are highly solvent exposed in the interacting region are also indicated [183].

Fig. 8. Selective observation of paramagnetic signals in ^{1}H-^{15}N spectra of the $[Fe_2S_2]^{2+}$-CIAPIN1 domain. The standard HSQC spectrum (red) is overlaid with the paramagnetic-tailored analogue (black) allowing to selectively observe signals from HN close in space to the paramagnetic center which usually escape detection in an standard experiment [184].

Fig. 9. NMR has been used to learn about the mitochondrial transfer of the $[Fe_2S_2]$ cluster from monothiol Glutaredoxin 5 (Grx5) to apoISCA1. (A) 1D ^{13}C NMR spectrum showing the iron binding cysteines in holo Grx5. The ^{13}C T_1 values of the identified CO and Cα signals are reported. (B) Scheme of the proposed transfer mechanism.

Fig. 10. Key structural elements of the ferritin nanocage. Top left: the subunits have a 4-helix bundle structure completed by a short helix at the C-term. Top right: pairs of subunit have extended contacts along C2 symmetry axes. Bottom left: C3 symmetry axes from where three subunits come in contact and form ion channels. Bottom right: C4 symmetry axes form when 4 subunits come in contact via their short C-term helices, creating hydrophobic channels. (Designed using PDB id 1MFR).

Fig. 11. Combined solution/solid state NMR approach for ferritin. Partial sequence specific assignment of ferritin spectra could be achieved via solid state NMR approaches and then transferred to solution spectra; the process was possible because the ^{13}C-^{13}C correlation maps in solution (blue) and solid state (red) are superimposable [209].

Fig. 12. Iron binding to ferritin. (A) The binding of iron to ferritin was monitored via solution ^{13}C-^{13}C NOESY [209]: when 2 iron/subunit are added (red trace) paramagnetic broadening beyond detection with respect to the apo form (black trace) is observed for a few signals (for example A26 and I144). (B) Paramagnetic effects at different stage of the titration with iron are mapped (red spheres) on the subunit structure. (C) The X-ray structure solved later on shows the di-ferric binding site which is fully consistent with the broadening observed with two iron/subunit [199].

Highlights

Brief history of paramagnetic NMR of iron sites in proteins

Application of NMR to protein-protein interactions

New NMR tools permit the fingerprinting of binding modules in transient iron sites

Trafficking of iron cofactors is mediated by protein-protein interactions

Sample cases are: ferritin, heme acquisition system and FeS assembly machineries

Figure 1

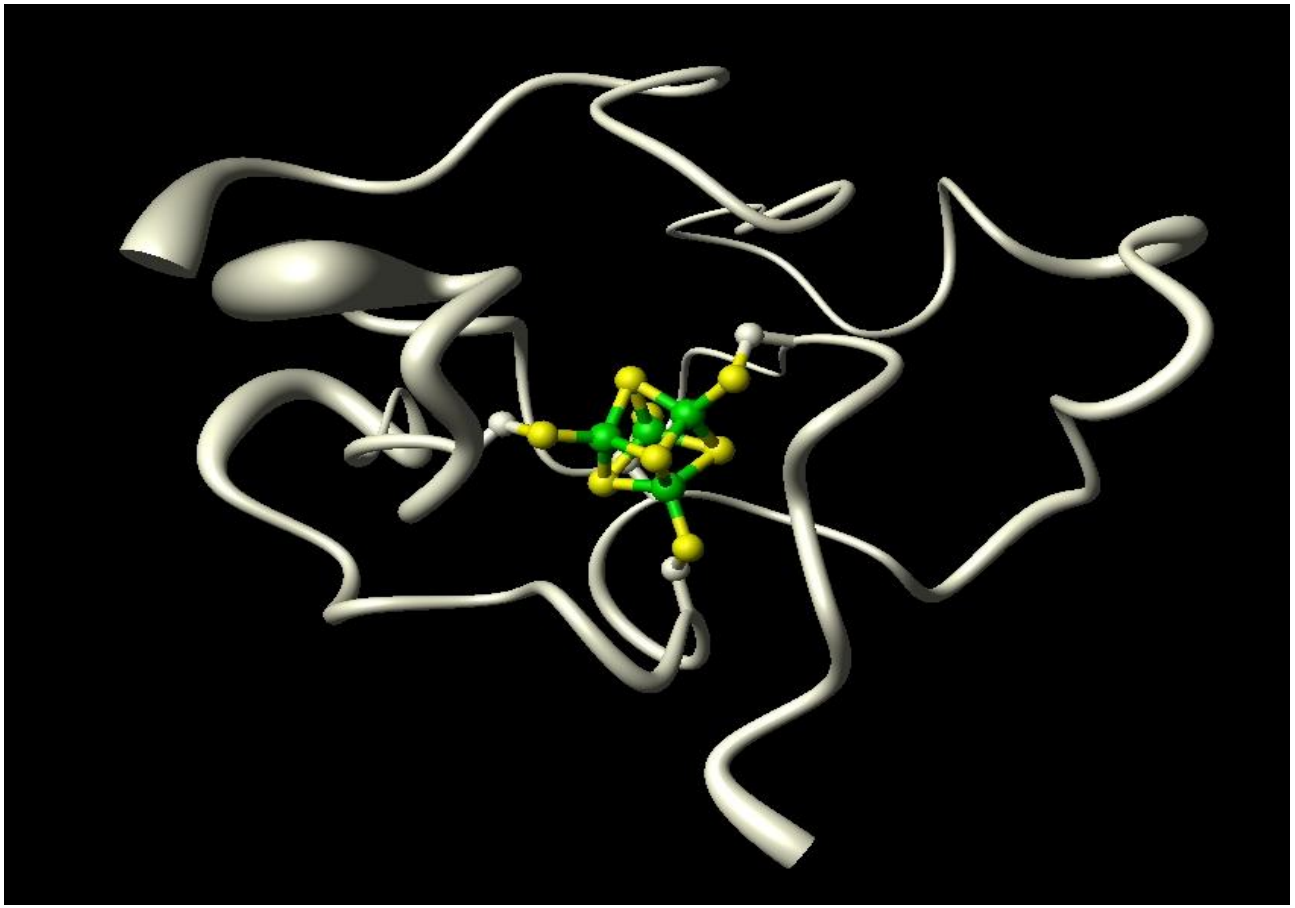

Figure 2

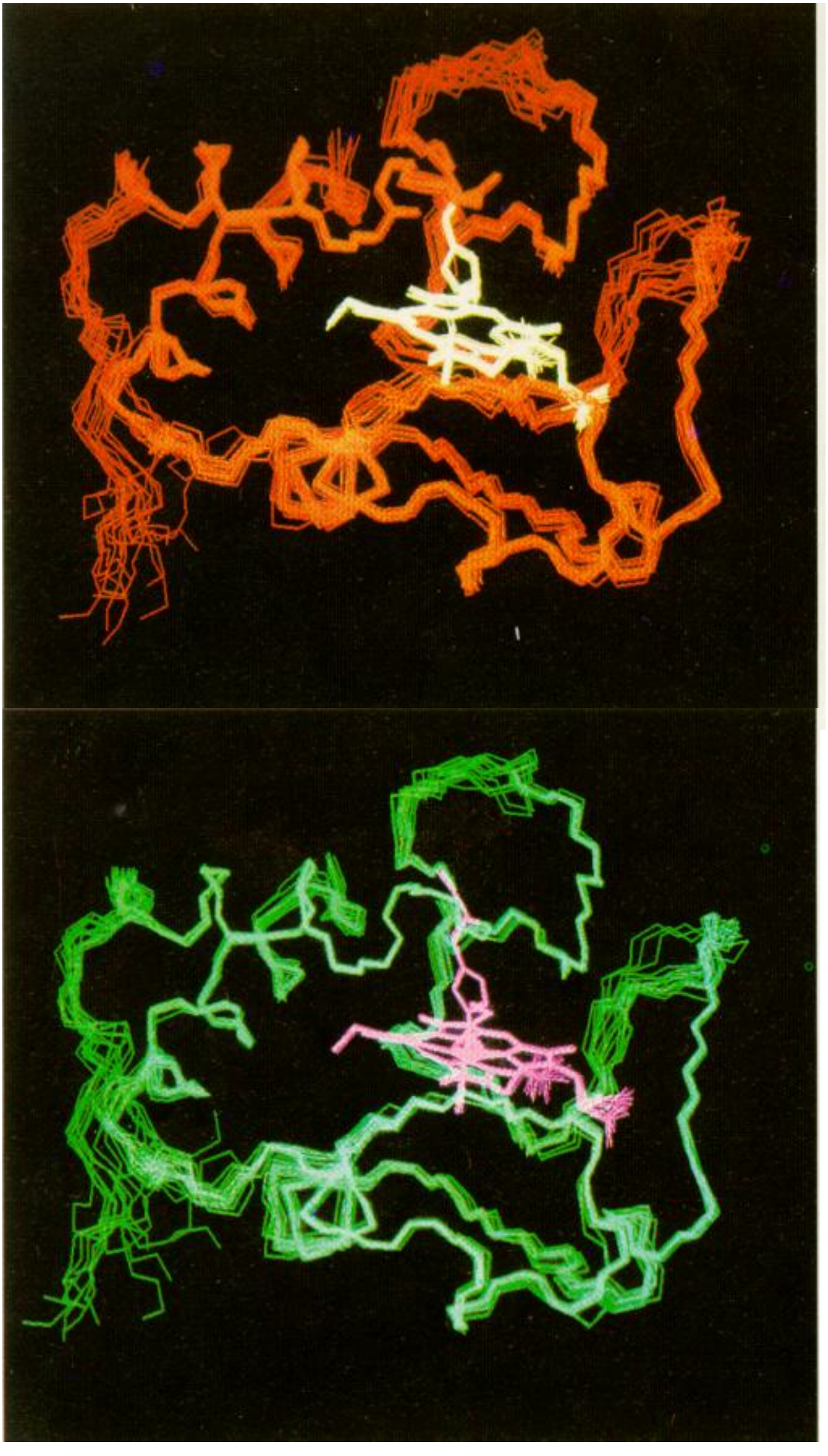

Figure 3

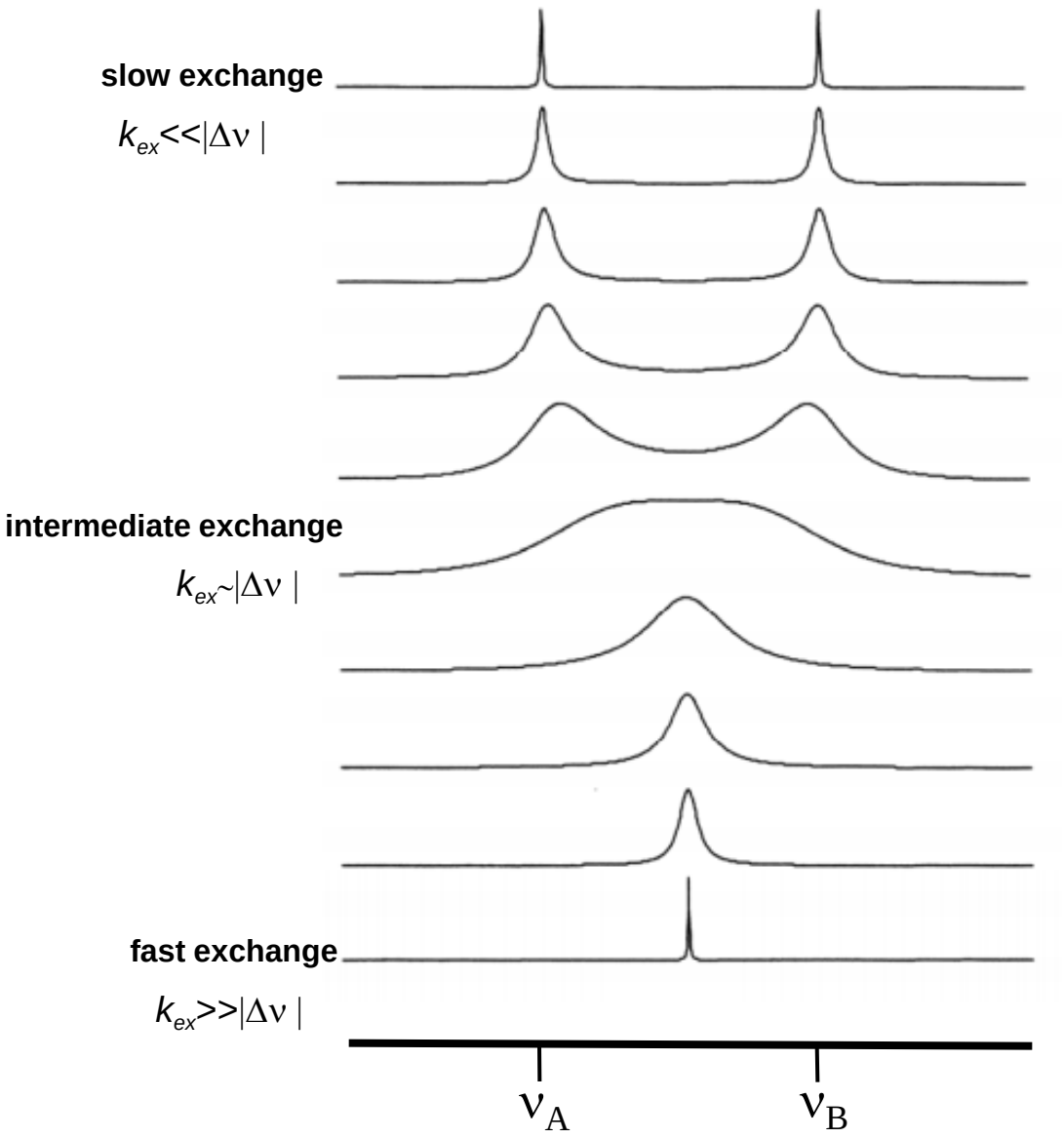
slow exchange
k_{ex}<<|Δν |
intermediate exchange
k_{ex}~|Δν |
fast exchange
k_{ex}>>|Δν |
ν_A
ν_B

Figure 4

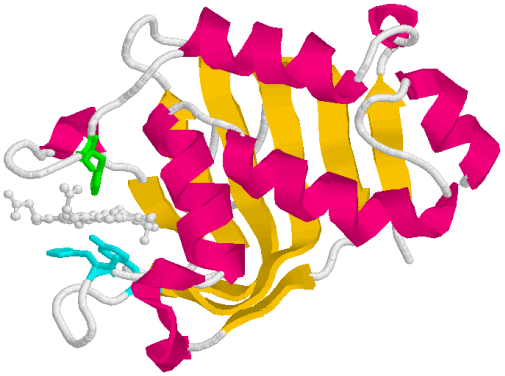

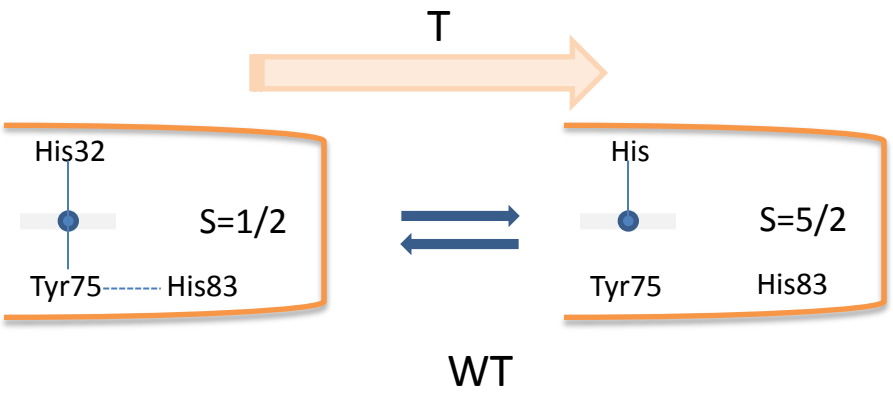
T
His32
S=1/2
Tyr75
His83
His
S=5/2
Tyr75
His83
WT

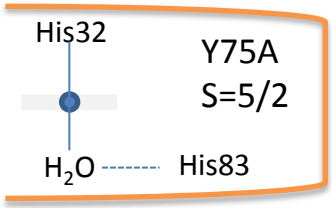
His32
Y75A
S=5/2
H2O
His83

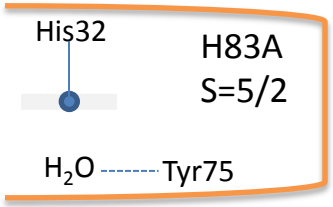
His32
H83A
S=5/2
H2O
Tyr75

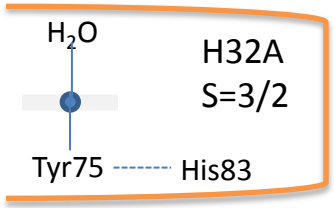
H2O
H32A
S=3/2
Tyr75
His83

Figure 5

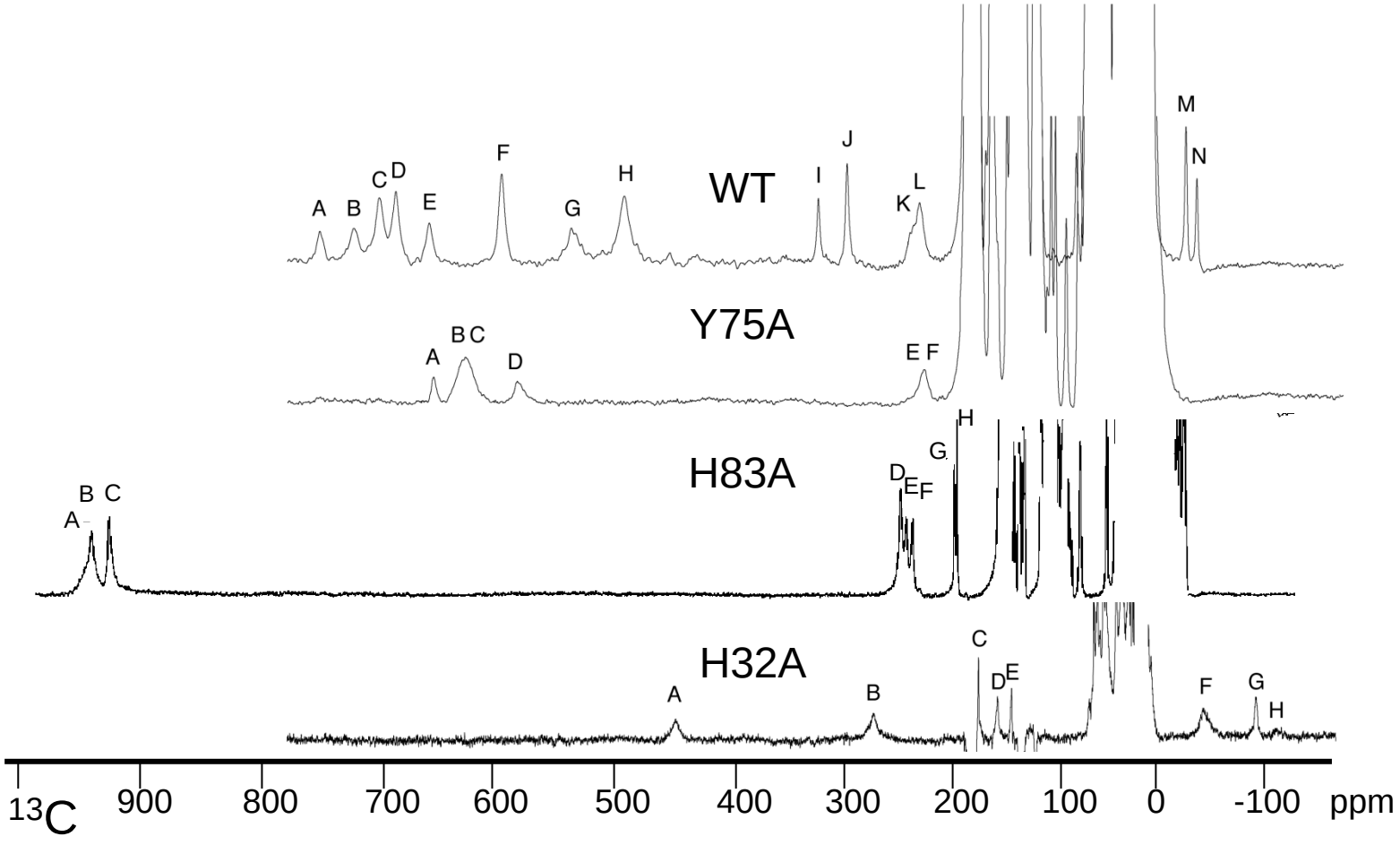
WT
A
B
C
D
E
F
G
H
I
J
K
L
M
N
Y75A
A
B C
D
E F
H83A
A
B
C
D
E
F
G
H
H32A
A
B
C
D
E
F
G
H
13C
900
800
700
600
500
400
300
200
100
0
-100
ppm

Figure 6

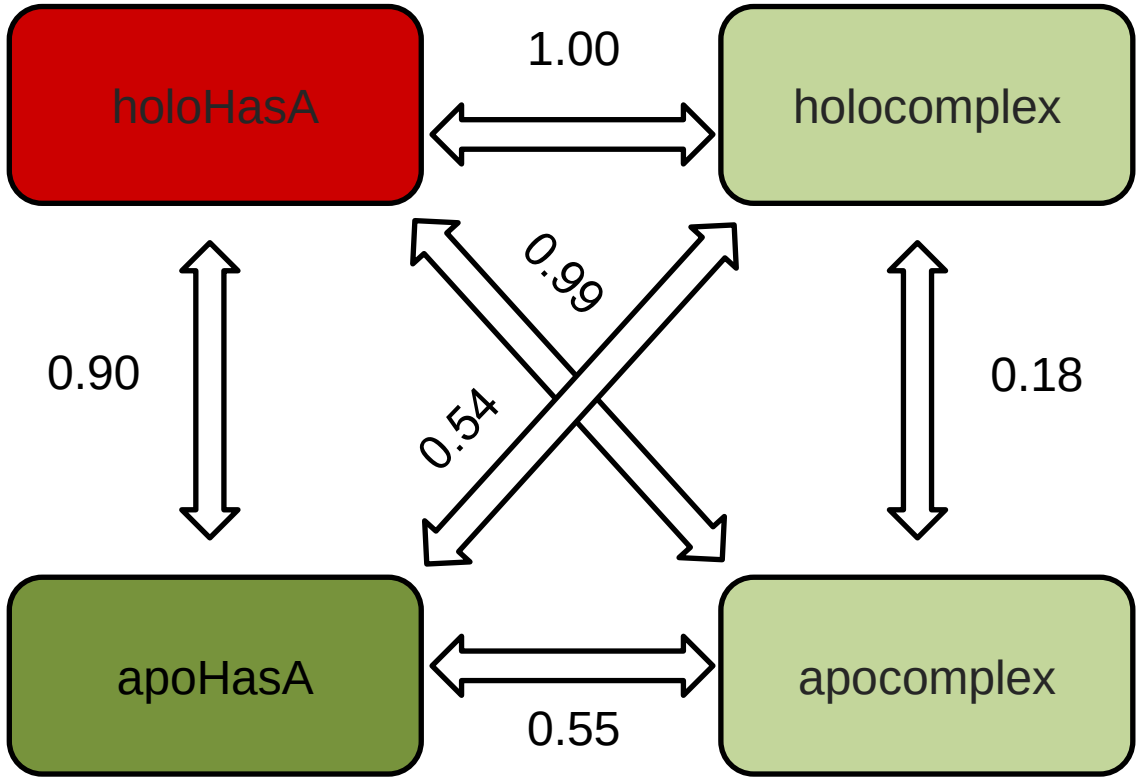
holoHasA
1.00
holocomplex
0.90
0.99
0.54
0.18
apoHasA
0.55
apocomplex

Figure 7

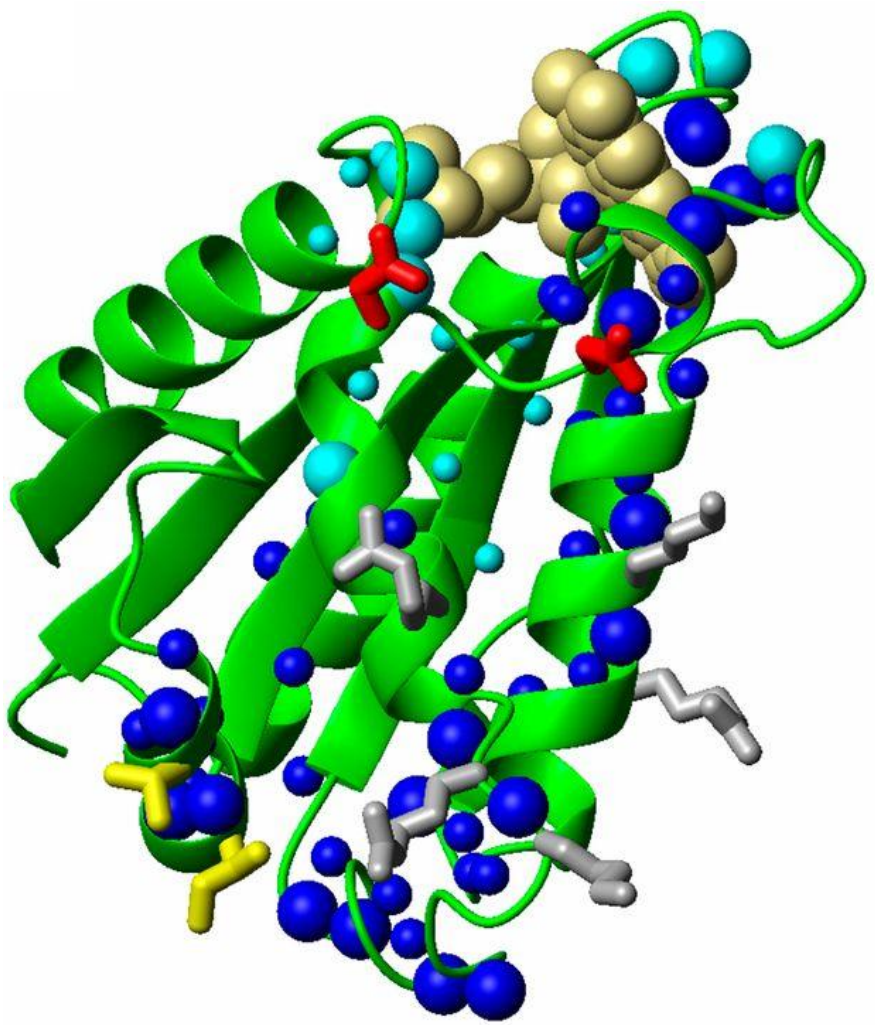

Figure 8

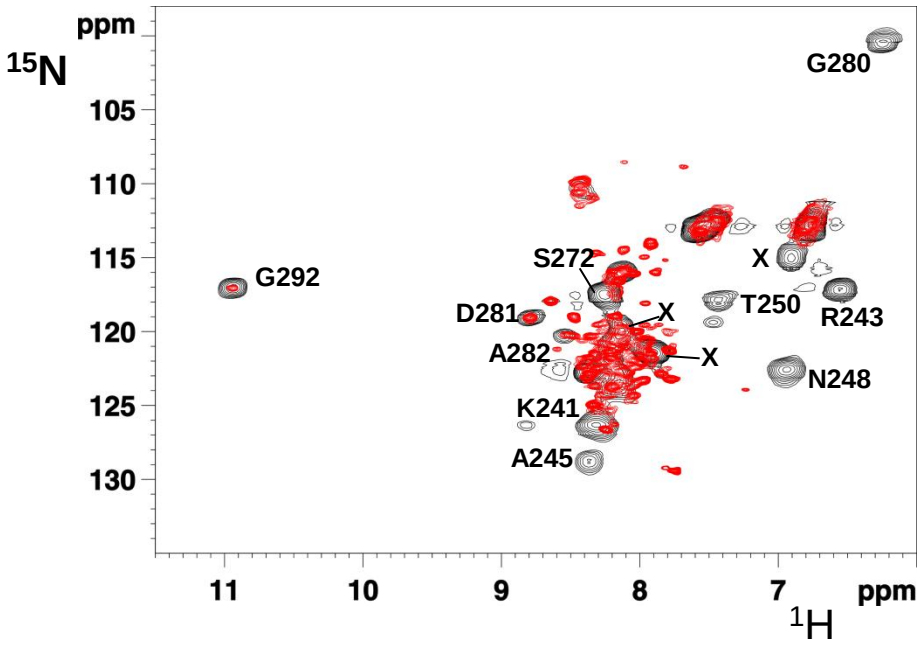
ppm
15N
105
110
115
120
125
130
G280
G292
S272
X
T250
R243
D281
X
A282
X
N248
K241
A245
11
10
9
8
7
ppm
1H

Figure 9

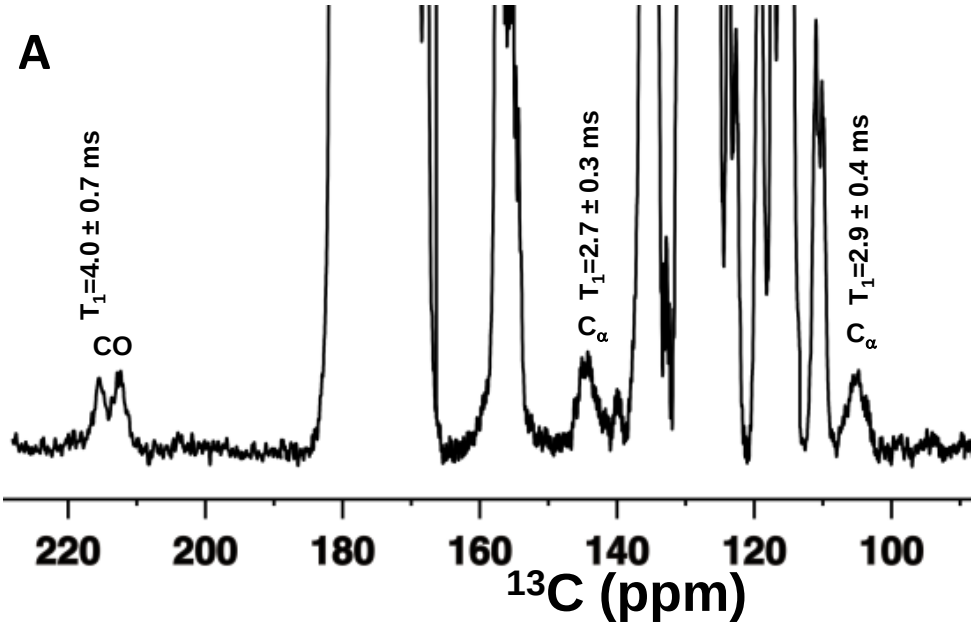
A
T1=4.0 ± 0.7 ms
CO
Cα T1=2.7 ± 0.3 ms
Cα T1=2.9 ± 0.4 ms
220
200
180
160
140
120
100
13C (ppm)

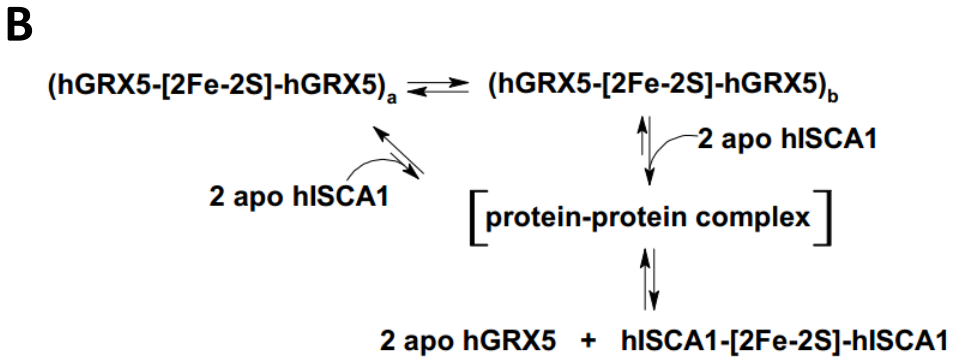
B
(hGRX5-[2Fe-2S]-hGRX5)a
(hGRX5-[2Fe-2S]-hGRX5)b
2 apo hISCA1
2 apo hISCA1
[protein-protein complex]
2 apo hGRX5 + hISCA1-[2Fe-2S]-hISCA1

Figure 10

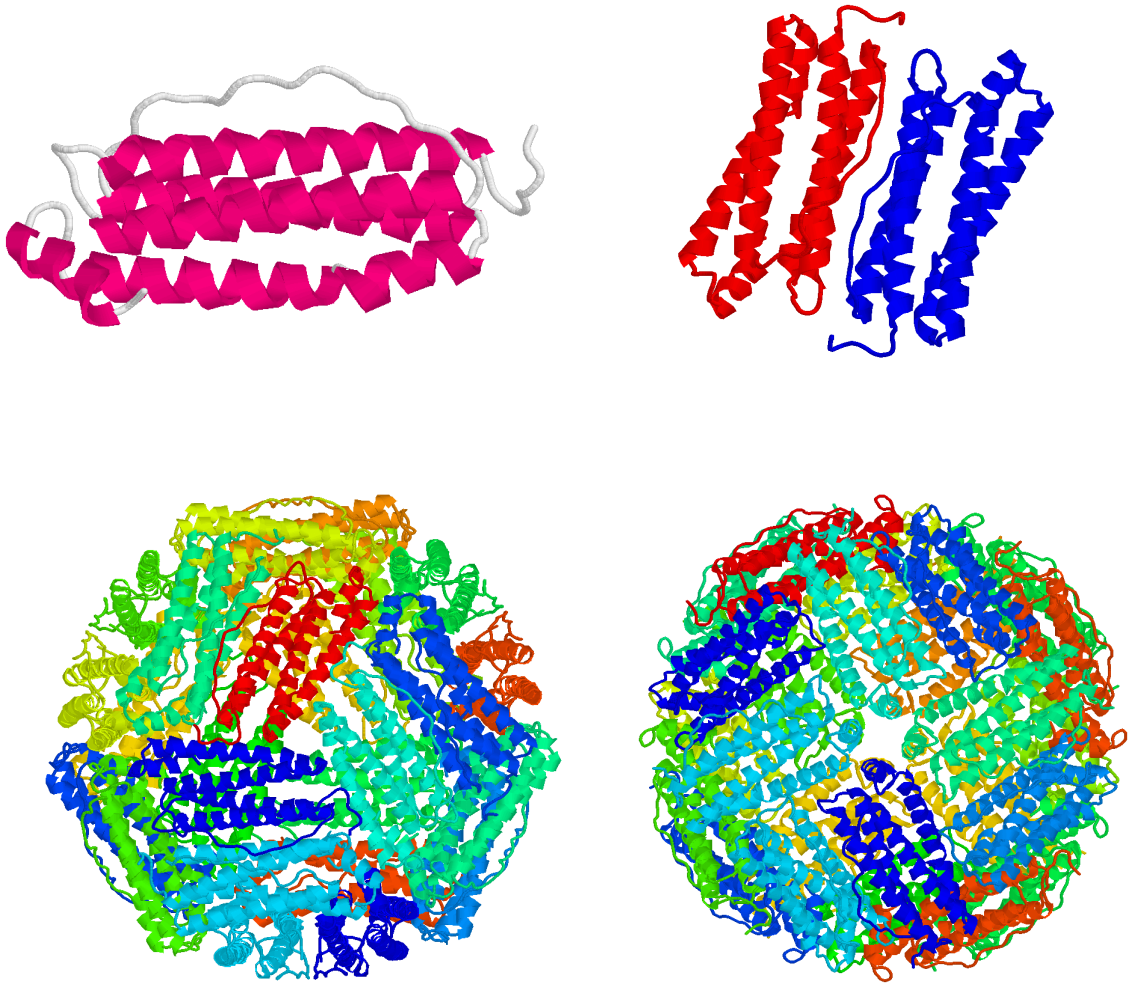

Figure 11

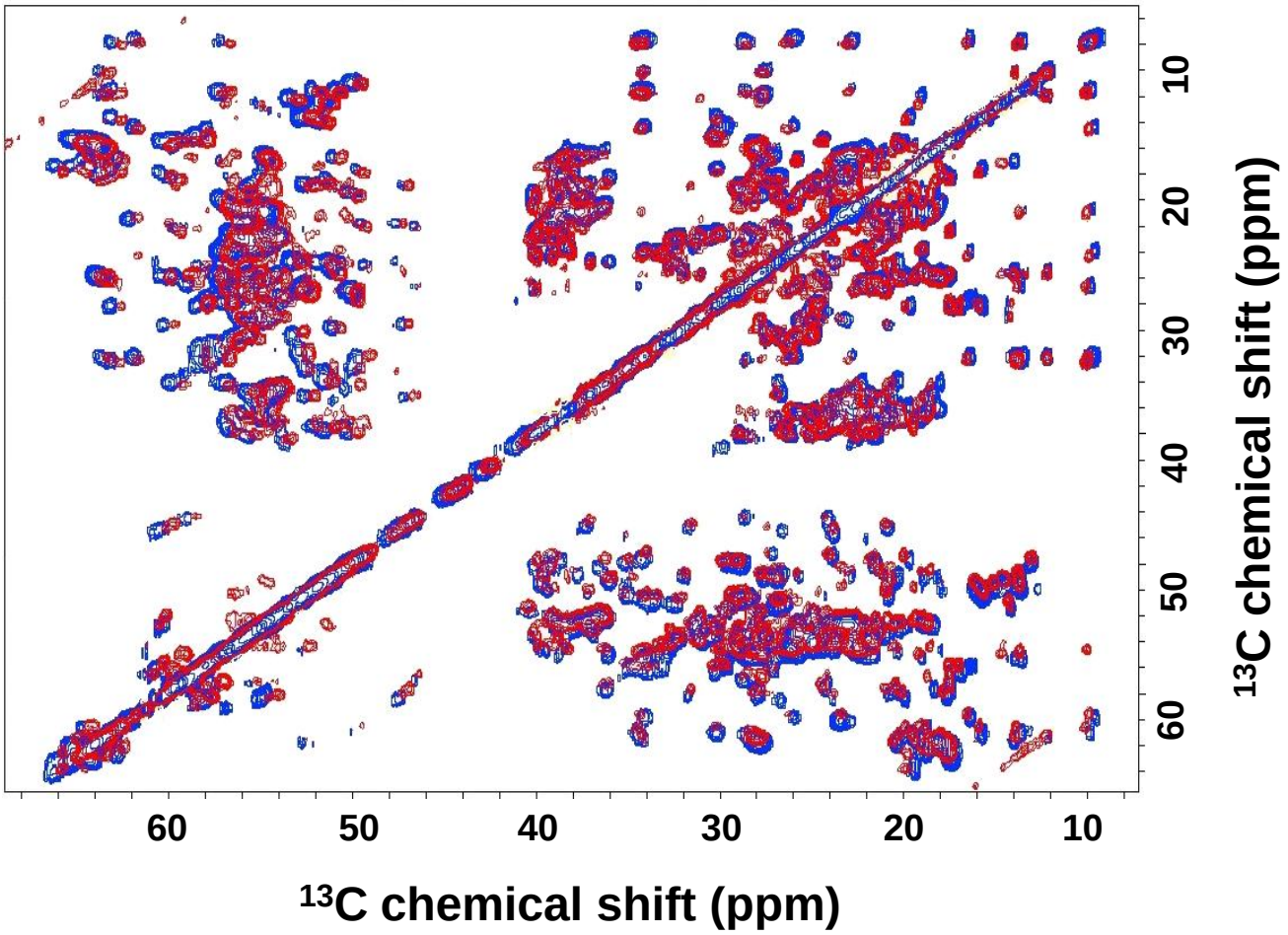
60
50
40
30
20
10
^{13}C chemical shift (ppm)
10
20
30
40
50
60
^{13}C chemical shift (ppm)

Figure 12

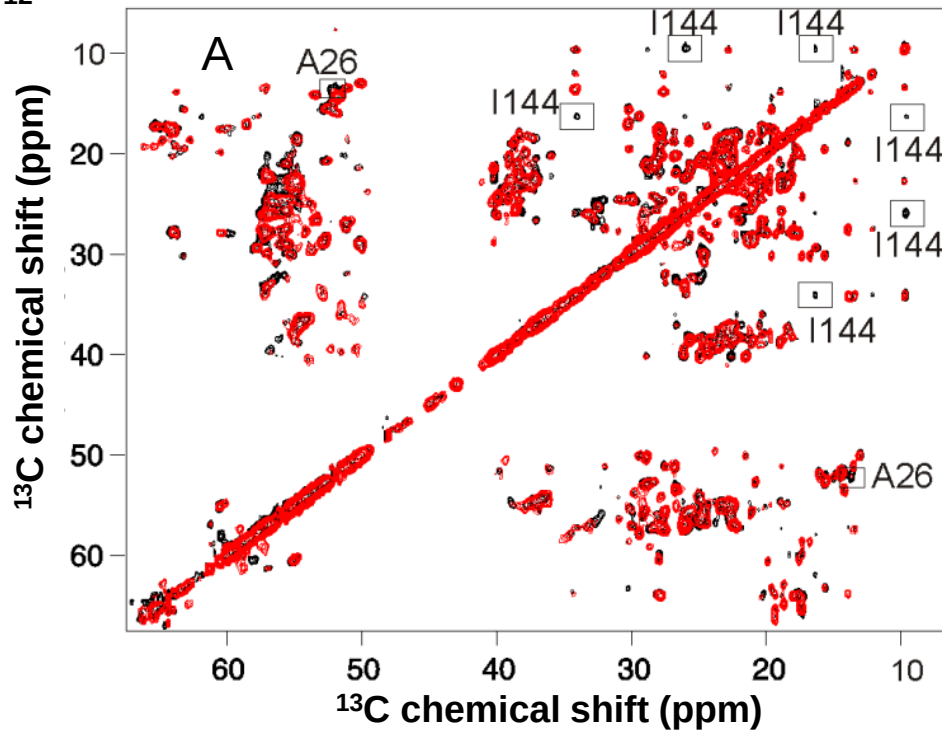
A
A26
I144
I144
I144
I144
I144
I144
A26
10
20
30
40
50
60
60
50
40
30
20
10
^{13}C chemical shift (ppm)
^{13}C chemical shift (ppm)

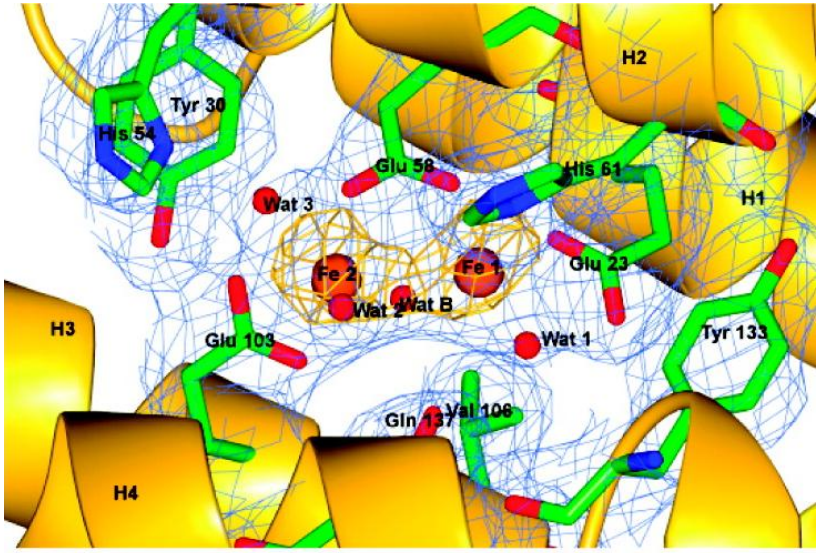
C
H2
Tyr 30
His 54
Glu 58
His 61
H1
Wat 3
Fe 2
Fe 1
Glu 23
Wat 2
Wat B
H3
Glu 103
Wat 1
Tyr 133
Gln 137
Val 106
H4

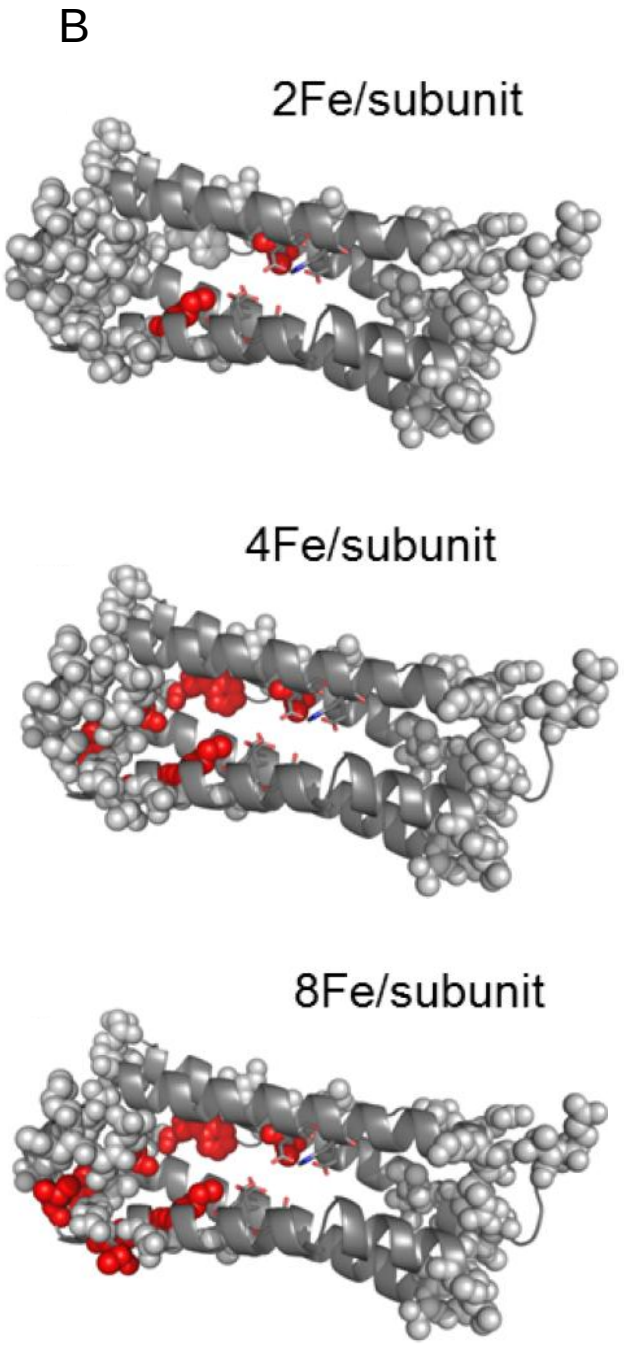
B
2Fe/subunit
4Fe/subunit
8Fe/subunit